is a novel tumor marker. *Biochem Biophys Res Commun.* 2003;306:16–25.
6. Nakatsura T, Komori H, Kubo T, et al. Mouse homologue of a novel human oncofetal antigen, glypican-3, evokes T-cell-mediated tumor rejection without autoimmune reactions in mice. *Clin Cancer Res.* 2004;10:8630–8640.
7. Komori H, Nakatsura T, Senju S, et al. Identification of HLA-A2- or HLA-A24-restricted CTL epitopes possibly useful for glypican-3-specific immunotherapy of hepatocellular carcinoma. *Clin Cancer Res.* 2006;12:2689–2697.
8. Lane TF, Sage EH. The biology of SPARC, a protein that modulates cell-matrix interactions. *FASEB J.* 1994;8:163–173.
9. Nakatsura T, Kageshita T, Ito S, et al. Identification of glypican-3 as a novel tumor marker for melanoma. *Clin Cancer Res.* 2004;10:6612–6621.
10. Ikuta Y, Nakatsura T, Kageshita T, et al. Highly sensitive detection of melanoma at an early stage based on the increased serum secreted protein acidic and rich in cysteine and glypican-3 levels. *Clin Cancer Res.* 2005;11:8079–8088.
11. O'Neill DW, Adams S, Bhardwaj N. Manipulating dendritic cell biology for the active immunotherapy of cancer. *Blood.* 2004;104:2235–2246.
12. Steinman RM, Banchereau J. Taking dendritic cells into medicine. *Nature.* 2007;449:419–426.
13. Murphy A, Westwood JA, Teng MW, et al. Gene modification strategies to induce tumor immunity. *Immunity.* 2005;22:403–414.
14. Kaplan JM, Yu Q, Piraino ST, et al. Induction of antitumor immunity with dendritic cells transduced with adenovirus vector-encoding endogenous tumor-associated antigens. *J Immunol.* 1999;163:699–707.
15. Motomura Y, Senju S, Nakatsura T, et al. Embryonic stem cell-derived dendritic cells expressing glypican-3, a recently identified oncofetal antigen, induce protective immunity against highly metastatic mouse melanoma, B16-F10. *Cancer Res.* 2006;66:2414–2422.
16. Fairchild PJ, Brook FA, Gardner RL, et al. Directed differentiation of dendritic cells from mouse embryonic stem cells. *Curr Biol.* 2000;10:1515–1518.
17. Senju S, Hirata S, Matsuyoshi H, et al. Generation and genetic modification of dendritic cells derived from mouse embryonic stem cells. *Blood.* 2003;101:3501–3508.
18. Matsuyoshi H, Senju S, Hirata S, et al. Enhanced priming of antigen-specific CTLs in vivo by embryonic stem cell-derived dendritic cells expressing chemokine along with antigenic protein: application to antitumor vaccination. *J Immunol.* 2004;172:776–786.
19. Matsunaga Y, Fukuma D, Hirata S, et al. Activation of antigen-specific cytotoxic T lymphocytes by beta2-microglobulin or TAP1 gene disruption and the introduction of recipient-matched MHC class I gene in allogeneic embryonic stem cell-derived dendritic cells. *J Immunol.* 2008;181:6635–6643.
20. Fujii S, Shimizu K, Kronenberg M, et al. Prolonged IFN-gamma-producing NKT response induced with alpha-galactosylceramide-loaded DCs. *Nat Immunol.* 2002;3:867–874.
21. Senju S, Iyama K, Kudo H, et al. Immunocytochemical analyses and targeted gene disruption of GTPBP1. *Mol Cell Biol.* 2000;20:6195–6200.
22. Niwa H, Masui S, Chambers I, et al. Phenotypic complementation establishes requirements for specific POU domain and generic transactivation function of Oct-3/4 in embryonic stem cells. *Mol Cell Biol.* 2002;22:1526–1536.
23. Niwa H, Yamamura K, Miyazaki J. Efficient selection for high-expression transfectants with a novel eukaryotic vector. *Gene.* 1991;108:193–199.
24. Hirata S, Senju S, Matsuyoshi H, et al. Prevention of experimental autoimmune encephalomyelitis by transfer of embryonic stem cell-derived dendritic cells expressing myelin oligodendrocyte glycoprotein peptide along with TRAIL or programmed death-1 ligand. *J Immunol.* 2005;174:1888–1897.
25. Hirata S, Matsuyoshi H, Fukuma D, et al. Involvement of regulatory T cells in the experimental autoimmune encephalomyelitis-preventive effect of dendritic cells expressing myelin oligodendrocyte glycoprotein plus TRAIL. *J Immunol.* 2007;178:918–925.
26. Watarai H, Nakagawa R, Omori-Miyake M, et al. Methods for detection, isolation and culture of mouse and human invariant NKT cells. *Nat Protoc.* 2008;3:70–78.
27. Bohm W, Thoma S, Leithauser F, et al. T cell-mediated, IFN-gamma-facilitated rejection of murine B16 melanomas. *J Immunol.* 1998;161:897–908.
28. Matsuyoshi H, Hirata S, Yoshitake Y, et al. Therapeutic effect of alpha-galactosylceramide-loaded dendritic cells genetically engineered to express SLC/CCL21 along with tumor antigen against peritoneally disseminated tumor cells. *Cancer Sci.* 2005;96:889–896.
29. Overwijk WW, Tsung A, Irvine KR, et al. gp100/pmel 17 is a murine tumor rejection antigen: induction of "self"-reactive, tumoricidal T cells using high-affinity, altered peptide ligand. *J Exp Med.* 1998;188:277–286.
30. Hyoudou K, Nishikawa M, Umeyama Y, et al. Inhibition of metastatic tumor growth in mouse lung by repeated administration of polyethylene glycol-conjugated catalase: quantitative analysis with firefly luciferase-expressing melanoma cells. *Clin Cancer Res.* 2004;10:7685–7691.
31. Hyoudou K, Nishikawa M, Kobayashi Y, et al. Inhibition of adhesion and proliferation of peritoneally disseminated tumor cells by pegylated catalase. *Clin Exp Metastasis.* 2006;23:269–278.
32. Wilson MT, Johansson C, Olivares-Villagomez D, et al. The response of natural killer T cells to glycolipid antigens is characterized by surface receptor down-modulation and expansion. *Proc Natl Acad Sci USA.* 2003;100:10913–10918.
33. Harada M, Seino K, Wakao H, et al. Down-regulation of the invariant Valpha14 antigen receptor in NKT cells upon activation. *Int Immunol.* 2004;16:241–247.
34. Hyoudou K, Nishikawa M, Kobayashi Y, et al. PEGylated catalase prevents metastatic tumor growth aggravated by tumor removal. *Free Radic Biol Med.* 2006;41:1449–1458.
35. Massi D, Franchi A, Borgognoni L, et al. Osteonectin expression correlates with clinical outcome in thin cutaneous malignant melanomas. *Hum Pathol.* 1999;30:339–344.
36. Infante JR, Matsubayashi H, Sato N, et al. Peritumoral fibroblast SPARC expression and patient outcome with resectable pancreatic adenocarcinoma. *J Clin Oncol.* 2007;25:319–325.
37. Sangaletti S, Stoppacciaro A, Guiducci C, et al. Leukocyte, rather than tumor-produced SPARC, determines stroma and collagen type IV deposition in mammary carcinoma. *J Exp Med.* 2003;198:1475–1485.
38. Alvarez MJ, Prada F, Salvatierra E, et al. Secreted protein acidic and rich in cysteine produced by human melanoma cells modulates polymorphonuclear leukocyte recruitment and antitumor cytotoxic capacity. *Cancer Res.* 2005;65:5123–5132.
39. Banchereau J, Palucka AK, Dhodapkar M, et al. Immune and clinical responses in patients with metastatic melanoma to CD34(+) progenitor-derived dendritic cell vaccine. *Cancer Res.* 2001;61:6451–6458.
40. Wang B, He J, Liu C, et al. An effective cancer vaccine modality: lentiviral modification of dendritic cells expressing multiple cancer-specific antigens. *Vaccine.* 2006;24:3477–3489.
41. Kavanagh B, Ko A, Venook A, et al. Vaccination of metastatic colorectal cancer patients with matured dendritic cells loaded with multiple major histocompatibility complex class I peptides. *J Immunother.* 2007;30:762–772.
42. Mendiratta SK, Thai G, Eslahi NK, et al. Therapeutic tumor immunity induced by polyimmunization with melanoma antigens gp100 and TRP-2. *Cancer Res.* 2001;61:859–863.
43. Nieda M, Okai M, Tazbirkova A, et al. Therapeutic activation of Valpha24+Vbeta11+ NKT cells in human subjects results in highly coordinated secondary activation of acquired and innate immunity. *Blood.* 2004;103:383–389.
44. Ishikawa A, Motohashi S, Ishikawa E, et al. A phase I study of alpha-galactosylceramide (KRN7000)-pulsed dendritic cells in

patients with advanced and recurrent non-small cell lung cancer. *Clin Cancer Res.* 2005;11:1910–1917.
45. Chang DH, Osman K, Connolly J, et al. Sustained expansion of NKT cells and antigen-specific T cells after injection of alpha-galactosyl-ceramide loaded mature dendritic cells in cancer patients. *J Exp Med.* 2005;201:1503–1517.
46. Uchida T, Horiguchi S, Tanaka Y, et al. Phase I study of alpha-galactosylceramide-pulsed antigen presenting cells administration to the nasal submucosa in unresectable or recurrent head and neck cancer. *Cancer Immunol Immunother.* 2008;57:337–345.
47. Senju S, Suemori H, Zembutsu H, et al. Genetically manipulated human embryonic stem cell-derived dendritic cells with immune regulatory function. *Stem Cells.* 2007;25: 2720–2729.
48. Fukuma D, Matsuyoshi H, Hirata S, et al. Cancer prevention with semi-allogeneic ES cell-derived dendritic cells. *Biochem Biophys Res Commun.* 2005;335:5–13.
49. Takahashi K, Tanabe K, Ohnuki M, et al. Induction of pluripotent stem cells from adult human fibroblasts by defined factors. *Cell.* 2007;131:861–872.

Oncogene (2009) 28, 662–673

www.nature.com/onc

ORIGINAL ARTICLE

Distinct role of ShcC docking protein in the differentiation of neuroblastoma

I Miyake[1], M Ohira[2], A Nakagawara[2] and R Sakai[1]

[1]*Growth Factor Division, National Cancer Center Research Institute, Tokyo, Japan and* [2]*Division of Biochemistry, Chiba Cancer Center Research Institute, Chiba, Japan*

The biological and clinical heterogeneity of neuroblastoma is closely associated with signaling pathways that control cellular characteristics such as proliferation, survival and differentiation. The Shc family of docking proteins is important in these pathways by mediating cellular signaling. In this study, we analysed the expression levels of ShcA and ShcC proteins in 46 neuroblastoma samples and showed that a significantly higher level of ShcC protein is observed in neuroblastomas with poor prognostic factors such as advanced stage and *MYCN* amplification ($P<0.005$), whereas the expression level of ShcA showed no significant association with these factors. Using TNB1 cells that express a high level of ShcC protein, it was demonstrated that knockdown of ShcC by RNAi caused elevation in the phosphorylation of ShcA, which resulted in sustained extracellular signal-regulated kinase activation and neurite outgrowth. The neurites induced by ShcC knockdown expressed several markers of neuronal differentiation suggesting that the expression of ShcC potentially has a function in inhibiting the differentiation of neuroblastoma cells. In addition, marked suppression of *in vivo* tumorigenicity of TNB1 cells in nude mice was observed by stable knockdown of ShcC protein. These findings indicate that ShcC is a therapeutic target that might induce differentiation in the aggressive type of neuroblastomas.
Oncogene (2009) **28,** 662–673; doi:10.1038/onc.2008.413; published online 10 November 2008

Keywords: Shc family; ERK; neuroblastoma; differentiation; RNAi

Introduction

Neuroblastoma is the most common pediatric solid tumor derived from the sympathoadrenal lineage of neural crest and its clinical and biological features are heterogeneous. Some types of neuroblastomas show favorable outcomes with spontaneous differentiation or regression by minimum treatment, whereas other types have malignant characteristics with metastasis and resistance to chemotherapy. Age of onset, tumor volume, presence of metastasis, pathological features and amplification of the *N-myc* gene are important prognostic factors of neuroblastoma. Previously, it was reported that the differential expression of Trk family receptors might contribute to clinical and biological outcomes of neuroblastomas (Nakagawara *et al.*, 1993; Nakagawara and Brodeur, 1997) whereas the cellular signaling involved in the regulation of the aggressiveness of neuroblastoma is largely unknown.

The Shc family of docking proteins is important in signaling pathways mediating the activation of various receptor tyrosine kinases (RTKs) such as the Trk family triggered by extracellular stimulations, to specific downstream molecules. The Ras–extracellular signal-regulated kinase (ERK) pathway and the phosphoinositide-3 kinase (PI3K)–Akt pathway are the most common signals regulated by Shc family proteins, representing important functions in cellular proliferation, survival and differentiation.

The Shc family has three members, ShcA/Shc, ShcB/Sli/Sck and ShcC/Rai/N-Shc encoded by different genes (Nakamura *et al.*, 1996; O'Bryan *et al.*, 1996; Pelicci *et al.*, 1996). ShcA protein having three protein isoforms, p46, p52 and p66, is ubiquitously expressed in most organs except the adult neural systems, whereas ShcC (p52 and p67 isoforms) are exclusively expressed in the neuronal system (Sakai *et al.*, 2000). In the central nervous system, ShcA expression is most significant during embryonic development with sudden decrease after birth. On the other hand, ShcC expression is remarkably induced around birth and maintained in the mature brain. The Shc family molecules have a unique PTB–CH1–SH2 modular organization with two phosphotyrosine-binding modules, PTB and SH2 domains, which recognize various phosphotyrosine-containing peptides with different specificities. CH1 domains contain several tyrosine phosphorylation sites that recruit other adaptor molecules such as Grb2. Functional analysis of ShcB and ShcC on the neuronal signal pathway indicate that these proteins in neuronal cells potentially regulate epidermal growth factor (EGF) or nerve growth factor (NGF) signaling in a similar fashion to ShcA (O'Bryan *et al.*, 1996; Nakamura *et al.*, 1998).

Major parts of neuroblastoma cell lines show the expression and tyrosine phosphorylation of ShcC protein, but its effect on the biology of tumor cells

Correspondence: Dr R Sakai, Growth factor Division, National Cancer Center Research Institute, Tsukiji, Chuo-ku, Tokyo 104-0045, Japan. E-mail: rsakai@ncc.go.jp
Received 9 May 2008; revised 3 September 2008; accepted 1 October 2008; published online 10 November 2008

remains to be elucidated. We have recently shown that constitutive tyrosine phosphorylation of ShcC is induced in a subset of neuroblastoma cells by the activation of anaplastic lymphoma kinase (ALK) owing to *ALK* gene amplification and the constitutively activated ALK–ShcC signal pathway could induce cell survival, anchorage-independent growth of the cells and progression of tumors (Miyake *et al*., 2002, 2005). In our study, significant amplification of *ALK* was observed in 3 of 13 neuroblastoma cell lines and in only 1 of 85 cases of human neuroblastoma samples (Osajima-Hakomori *et al*., 2005). Considering these results, it was suspected ShcC might also contribute to the signal pathway associated with the tumor behavior in ALK-independent manners in majority of neuroblastoma cells.

In a recent report, high expression of ShcC mRNA was shown to be a poor prognostic factor in neuroblastoma patients through the semiquantitative reverse transcriptase -PCR analysis of tissue samples (Terui *et al*., 2005), suggesting the possibility that ShcC protein might be causative of tumor progression in neuroblastoma patients. In the current study, we examined the expression levels of ShcC protein in tumor samples of 46 neuroblastoma patients and confirmed the significant association of the expression levels of ShcC protein with several factors linked to unfavorable outcome of neuroblastoma. Furthermore, we investigated the functions of ShcC in cell proliferation, differentiation and *in vivo* tumorigenicity of neuroblastoma cells by knockdown of ShcC expression in neuroblastoma cell lines expressing a high level of ShcC without *ALK* amplification.

Results

Expression and tyrosine phosphorylation of ShcC in neuroblastoma cell lines

At first, the expression of ShcA and ShcC was analysed in 11 neuroblastoma cell lines using each specific antibody (Supplementary Figure A) along with DLD-1 as a control, which is known to express ShcA protein (mainly p46ShcA and p52ShcA), but not ShcC protein (Figure 1a). The three cell lines with *ALK* gene amplification (NB-39-v, Nagai and NB-1: Group A) expressed ShcC at a moderate level in contrast to their significant phosphorylation so that ALK–ShcC complex is mediating the dominant oncogenic signal (Miyake *et al*., 2002; Osajima-Hakomori *et al*., 2005). Other

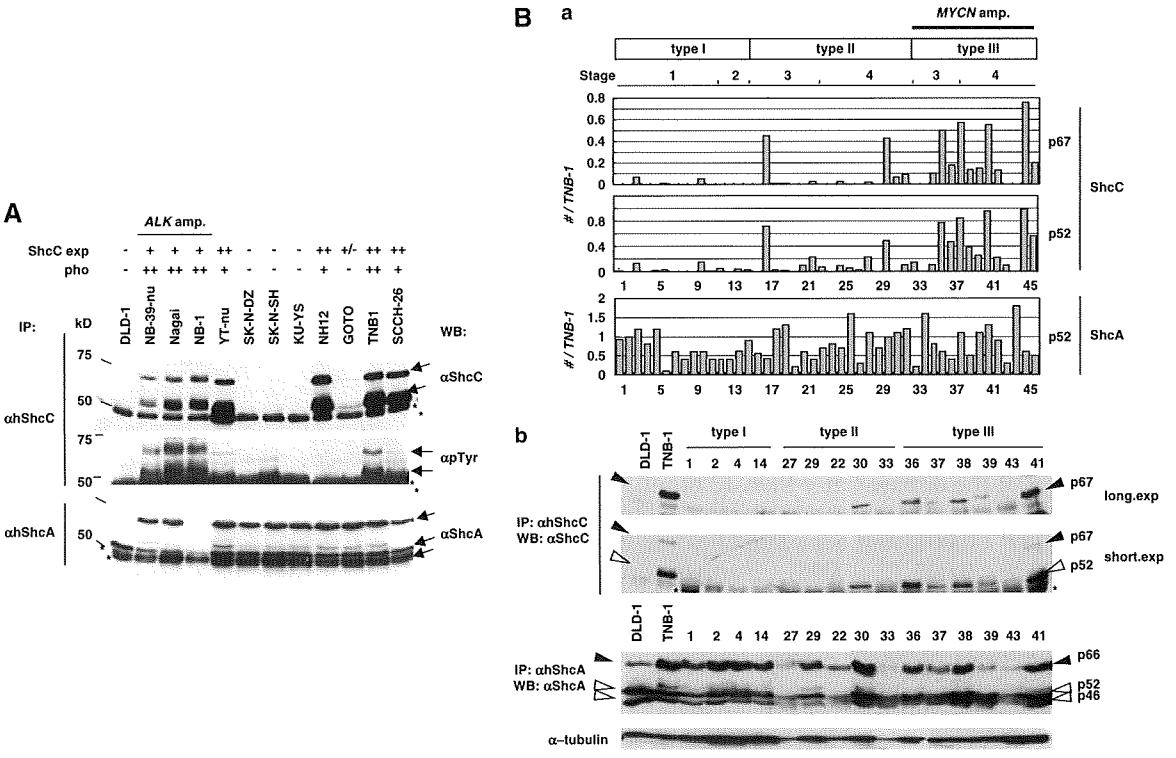

Figure 1 (**A**) Expression and tyrosine phosphorylation of ShcC in neuroblastoma cell lines detected by specific antibody. The expression of ShcA (lower panel), ShcC (upper panel) and tyrosine phosphorylation of ShcC was analysed in 11 neuroblastoma cell lines including the cell lines with anaplastic lymphoma kinase (*ALK*) gene amplification (*ALK* amp.) along with DLD-1 as a control. Lysates were immunoprecipitated and then immunoblotted with antibodies against the indicated molecules. The levels of expression/phosphorylation of ShcC are indicated above. Asterisks show heavy chains of immunoglobulin. Positions of molecular mass markers (kDa) are shown to the left. (**B**) Expression of ShcC and ShcA in the tissue samples of three subsets of neuroblastoma patients. (a) Expression levels of ShcC/ShcA in the samples of 46 neuroblastoma patients were detected by western blotting being compared to the level of expression in TNB-1 cells (= 1.0) as an internal control among each experiment and was corrected by each expression level of a-tubulin. (b) Expression of ShcC (upper panel)/ShcA (middle panel) of representative samples of each subset were detected on a filter. The exposure time of the filter onto X-ray films was different to detect between p52ShcC (short exposure: lower panel) and p67ShcC (long exposure: upper panel). Each isoform of ShcC/ShcA is indicated by opened or filled triangles. Asterisks show heavy chains of immunoglobulin.

neuroblastoma cells with a single copy of the *ALK* gene were divided into two groups, one with considerably high levels of ShcC expression (YT-v, NH-12, TNB-1 and SCCH-26: Group B) and the other with almost no ShcC expression (KU-YS, SK-N-DZ, SK-N-SH and GOTO: Group C). Most of the cells in the Group B showed a morphological tendency to aggregate each other and rather low adhesion to the culture plate, compared with the cells of the Group C (data not shown). The degrees of ShcC phosphorylation in the cells in Group B appeared to be lower than the cells with *ALK* amplification (Figure 1A, middle panel). In contrast to ShcC, the expression of ShcA was within similar levels among neuroblastoma cell lines (Figure 1A, lower panel).

The expression level of ShcC is prominent in tissue samples of poor risk neuroblastoma patients

Next we analysed the expression of ShcA and ShcC protein in 46 primary human neuroblastoma specimens using each specific antibody. These tissue samples were classified into three subsets using Brodeur's classification; type I (stage 1, 2 or 4S; a single copy of *MYCN*), type II (stage 3 or 4; a single copy of *MYCN*) and type III (all stages; amplification of *MYCN*) (Brodeur and Nakagawara, 1992; Ohira *et al*., 2003). The expression level of ShcA and ShcC in western blotting was standardized by intensity of α-tubulin within each filter, standardized by the amounts in TNB-1 cells as an internal control among different filters and statistically evaluated from at least two independent western blots for each sample (Table 1). We found that there is a significant difference in the expression levels of ShcC among the subsets of neuroblastomas. In the group of type II and type III, the expression level of ShcC protein was substantially higher than that in the type I group (Figure 1Ba). Both isoforms of ShcC, p52ShcC and p67ShcC, showed similar patterns of expression. As shown in Table 2, the expression level of ShcC has a significant correlation with several clinical factors including late onset of the disease (later than 12 months) (p52/p67: $P<0.001/P=0.015$), advanced clinical stage (stages III and IV) ($P<0.001$) and gene amplification of *MYCN* (p52/p67: $P<0.002/P=0.005$). Furthermore, most of the samples from the patients who died within 12 months after the onset of the disease showed significantly higher levels of ShcC expression than the other group of samples in which patients lived longer than 12 months (p52/p67: $P=0.006/P=0.009$). In contrast, variable expression levels of both isoforms of ShcA protein, p52 and p66, were observed in neuroblastoma samples with no significant difference among three subsets of clinical group ($P>0.05$) (Table 2; Figure 1Ba). The results of representative samples from each subset are shown in Figure 1Bb. These data indicate that the expression of ShcC protein is significantly associated with multiple prognostic factors of neuroblastoma, suggesting that ShcC has specific functions in malignant phenotypes of neuroblastoma presumably by modulating cellular signaling.

Biological effects of ShcC downregulation on TNB-1 cells

To elucidate the biological functions of ShcC in the tumor characteristics causing unfavorable outcomes of neuroblastoma patients, we investigated the effects of ShcC knockdown on the cellular biology and signal transduction in one of the neuroblastoma cell lines, TNB-1, which expresses a high level of ShcC protein with no *ALK* amplification. The expression of ShcC and ShcA was suppressed by RNA interference using two independent sets of specific small interfering RNA (siRNA) oligonucleotides corresponding to ShcC and ShcA, respectively (Figure 2Aa). The growth rate of TNB-1 cells transfected with the ShcA siRNA was severely suppressed (Figure 2Ab), owing to impaired ability of proliferation and survival, which is consistent with previous reports (Ravichandran, 2001). ShcC-knockdown cells showed a relatively weak effect on growth rate in the normal culture condition (Figure 2Ab).

Downregulation of ShcC induces neurite outgrowth and increases differentiation-related markers in TNB-1 cells

ShcC knockdown caused morphological changes to rather flat and spindle shape and neurite extension within 24 h after transfection of ShcC siRNA (Figure 2Ba). These neurite-bearing cells express higher amount of microtubule-associated protein 2 (MAP-2), growth-associated protein 43 (GAP-43), a protein expressed in the growing neurites, and chromogranin A (Chr-A; Figure 2Bb), markers of neuronal differentiation (Giudici *et al*., 1992) than the control cells. On the other hand, TNB-1 cells treated with ShcA siRNAs showed no remarkable change compared with the control cells, relatively round with small processes attached to the dish surface (Figure 2Ba). These results suggest that the endogenous ShcC negatively affects neurite outgrowth and differentiation of TNB-1 cells.

Persistent activation of ERK1/2 due to ShcC downregulation induces neurite outgrowth in TNB-1 cells

Neuronal differentiation is closely associated with mitogen-activated protein kinase (MAPK)/ERK kinase (MEK)/ERK and PI3K–AKT pathways and both of them might be controlled downstream of Shc family signaling. Downregulation of ShcA induced the suppression of extracellular signal-related kinase 1/2 (ERK1/2) and AKT pathways at 48 h after transfection of siRNA, nevertheless ShcC downregulation apparently elevated the base level of ERK phosphorylation and slightly enhanced AKT activation (Figure 3a). This elevation of ERK phosphorylation sustained until 96 h after transfection of siRNA. Similar effect on the ERK activation was also observed in NH-12 and YT-v cells, which express high amount of ShcC (Supplementary Figure B). It is reported that sustained activation of ERK is responsible for neurite outgrowth and differentiation of PC12 cells (Qui and Green, 1992). To investigate whether neuronal extension of TNB-1 cells by ShcC RNAi was induced by sustained activation of ERK, the effect of MEK inhibitor, PD98059, on the

Table 1 Characteristics of 46 neuroblastoma samples

Case	*Type*	*Stage*	*Age (months)*	*MYCN*	*Prognosis*	*p52ShcC*	*p67ShcC*	*p52ShcA*	*p66ShcA*
1	I	1	8	1	A	0.01	0	0.92	0.58
2		1	7	1	A	0	0	0.92	0.52
3		1	8	1	A	0.13	0.07	1.16	0.58
4		1	1	1	A	0	0	0.81	0.63
5		1	4	1	A	0.013	0	1.26	0.62
6		1	8	1	A	0.03	0.006	0.81	0.60
7		1	8	1	A	0	0	0.54	0.70
8		1	7	1	A	0	0	0.40	0.48
9		1	9	1	A	0	0	0.40	0.58
10		1	7	1	A	0.15	0.05	0.42	0.31
11		1	7	1	A	0.003	0	0.35	0.36
12		2	38	1	A	0.047	0	0.41	0.20
13		2	7	1	A	0	0	0.40	0.39
14		2	7	1	A	0.038	0	0.60	0.63
15		2	>132	1	A	0.03	0	0.83	0.62
16	II	3	8	1	A	0	0	0.56	0.45
17		3	7	1	A	0.72	0.45	0.42	0.49
18		3	7	1	A	0.03	0.01	1.2	0.62
19		3	8	1	A	0.015	0.01	1.3	0.67
20		3	23	1	A	0	0	0.25	0.32
21		3	22	1	A	0.10	0	0.63	0.63
22		3	>108	1	A	0.23	0.03	0.45	0.36
23		3	18	1	A	0.074	0.025	0.75	0.45
24		3	47	1	A*	0	0.03	0.87	0.65
25		3	21	1	D	0.089	0.03	0.76	0.56
26		3	96	1	A*	0.054	0.001	1.6	0.54
27		4	5	1	A	0.03	0	1.03	0.28
28		4	55	1	A	0.22	0.018	1.14	0.33
29		4	4	1	A	0	0	0.52	0.49
30		4	22	1	D	0.49	0.43	0.89	0.48
31		4	45	1	A*	0	0.068	1.17	0.53
32		4	57	1	A*	0.10	0.093	1.2	0.42
33		4	102	1	A*	0.15	0	1.5	0.49
34	III	3	32	amp	A*	0	0	1.6	0.37
35		3	13	amp	D	0.11	0.10	0.86	0.53
36		3	33	amp	D	0.77	0.50	0.64	0.50
37		3	21	amp	A*	0.47	0.18	0.47	0.49
38		3	26	amp	A*	0.84	0.57	1.1	0.58
39		4	23	amp	D	0.38	0.13	0.99	0.35
40		4	7	amp	D	0.25	0.15	1.1	0.58
41		4	>132	amp	D	0.96	0.55	1.32	0.65
42		4	18	amp	D	0.22	0.13	0.99	0.63
43		4	>24	amp	D	0.10	0	0.76	0.54
44		4	59	amp	D	0	0	1.80	0.85
45		4	30	amp	D	0.99	0.76	0.60	0.56
46		4	34	amp	D	0.56	0.21	0.53	0.47

Type, as described in 'Materials and methods'; age: onset of the disease (months); stage, INSS stage; MYCN, single copy (1) or amplification (amp) of *MYCN* gene; prognosis, alive (A) or death (D) within 12 months after diagnosis; A*, death after 12 months from diagnosis; p52/p67 ShcC and p52/66 ShcA, the intensity of each band obtained by western analysis, standardized according to control signals, such as the bands of TNB-1 and α-tubulin as described in 'Materials and methods'.

differentiation of TNB-1 cells by knockdown of ShcC was examined. It was found that inhibition of the ERK pathway abolished the neurite outgrowth of TNB-1 cells by ShcC knockdown, indicating that ShcC protein has the potential to suppress neurite outgrowth which is dependent on the sustained activation of the ERK pathway (Figure 3b). In addition, the sustained activation of ERK by the expression of activated Raf protein, RafCAAX (Leevers *et al.*, 1994; Stokoe *et al.*, 1994) also induced neurite outgrowth in TNB-1 cells (Supplementary Figure C) just as in PC12 cells (Dhillon *et al.*, 2003). We also analysed the effect of PI3K inhibitor on neurite outgrowth induced by ShcC RNAi to check the involvement of the PI3K–AKT pathway, whereas no apparent effects on the number and length of the neurite extension were observed (Supplementary Figure D).

Effect of ShcC knockdown on ERK activation is enhanced by collagen stimulation by ShcA–Grb2 signaling

Among several culture conditions of cells examined for the effect of ShcC RNAi on the activity of ERK, the most obvious activation of ERK was observed after the

Table 2 Correlation between the expression of ShcC protein and identified prognostic factors of neuroblastoma

	p52		*p67*	
	Average	*t-Test*	*Average*	*t-Test*
ShcC				
Age (months)				
12>	0.071		0.037	
>12	0.27	**<0.001**	0.18	0.015
Stage				
I–II	0.03		0.0084	
III–IV	0.26	**<0.001**	0.14	**<0.001**
MYCN				
Single	0.083		0.040	
amp.	0.43	**0.002**	0.25	**0.005**
Death in 12 months				
–	0.10		0.047	
+	0.41	**0.006**	0.25	**0.009**
	p52		*p66*	
	Average	*t-Test*	*Average*	*t-Test*
ShcA				
Age (months)				
12>	0.72		0.53	
>12	0.82	0.2	0.52	0.32
Stage				
I–II	0.68		0.52	
III–IV	0.82	0.1	0.52	0.22
MYCN				
Single	0.73		0.51	
amp.	0.88	0.16	0.55	0.16
Death in 12 months				
–	0.75		0.50	
+	0.84	0.27	0.57	0.11

Expression levels of ShcC and ShcA in tissue samples from 46 neuroblastoma patients quantified were analyzed statistically using *t*-test. The variables compared are age, onset of the disease (months); stage, INSS stage; MYCN, single copy or amplification of *MYCN* gene. Statistically significant correlation ($P<0.01$) is indicated in bold.

cells were plated on collagen dishes following suspending condition (Figure 4a, lower panel). On the contrary, the activation level of ERK due to ShcC RNAi was not significant in the suspending condition (Supplementary Figure E, left panel) showing that ShcC RNAi-induced ERK activation depends on attachment to the specific extracellular matrix (ECM).

In contrast, ERK activation was consistently suppressed by knockdown of ShcA regardless of these culture conditions (Figure 4a, upper panel).

Integrins-mediated extracellular signaling lead the activation of Ras/ERK signaling by ShcA, and that process is reported to be associated with Src family kinase (Wary *et al*., 1996, 1998), focal adhesion kinase (Hecker *et al*., 2002) or some RTKs (Moro *et al*., 1998; Hinsby *et al*., 2004). In TNB-1 cells, enhanced ShcA phosphorylation and ShcA–Grb2 complex formation was observed following collagen stimulation and further increased by ShcC RNAi (Figures 4b and c). To examine whether the phosphorylation of ShcA is necessary for the neurite formation, the effect of double knockdown of both ShcC and ShcA was examined in TNB-1 cells. ERK activation and neurite outgrowth were not detected in the absence of both ShcC and ShcA, indicating that ShcC RNAi-induced neurite outgrowth of TNB-1 cells might be dependent on the ShcA expression in adherent state (Figure 4d).

Expression of ShcC suppresses the phosphorylation of ShcA in KU-YS cells stimulated by EGF

To further analyse the effects of ShcC expression on ShcA phosphorylation in neuroblastoma cells, we introduced a vector expressing p52ShcC into KU-YS neuroblastoma cells, which do not express a detectable amount of endogenous ShcC protein (Figure 1A), and obtained several stable clones expressing p52ShcC at different levels (Figure 5a). As controls, clones overexpressing p46/p52ShcA, or expressing the expression vector alone were also prepared. We checked the ShcA phosphorylation of each clone under the stimulation of EGF (Figure 5b). EGF stimulation to the control and ShcA expressing cells showed typical activation of ShcA, whereas the cell expressing ShcC showed decreased levels of ShcA phosphorylation according to the levels of ShcC protein. We also confirmed that activation of ShcA by EGF was suppressed in the cells transiently overexpressing ShcC (Supplementary Figure F). Those cells showed almost the same level of EGF receptor (EGFR) activation induced by EGF, judging from the phosphorylation levels of EGFR indicating that the expression of ShcC negatively affected the EGFR–ShcA signaling after the activation of EGFR, such as competing manners against ShcA. In addition, we examined whether tyrosine phosphorylation of ShcC is crucial for the suppression of ShcA phosphorylation by establishing two clones that express a p52ShcC mutant, 3YF lacking all three tyrosines, which are reported to be involved in the tyrosine phosphorylation of ShcC (Miyake *et al*., 2005). It was revealed that the 3YF mutant of ShcC could suppress the EGF-induced activation of ShcA in both clones almost as efficiently as the original ShcC in ShcC2 cells (Supplementary Figure G), suggesting that negative regulation of ShcA phosphorylation by ShcC does not require tyrosine phosphorylation of ShcC.

ShcC downregulation negatively affects anchorage-independent growth and in vivo *tumorigenicity*

We investigated the effect of ShcC knockdown on the anchorage-independent growth and *in vivo* tumorigenicity of TNB-1 cells by establishing cells with stable suppression of ShcC expression using the miR RNAi expression vector (as described in 'Materials and methods'). As analysed in the mixed clones by soft agar colony formation assay; stable suppression of ShcC caused marked inhibition of anchorage-independent growth (Figure 6a). Three isolated clones of ShcC miR

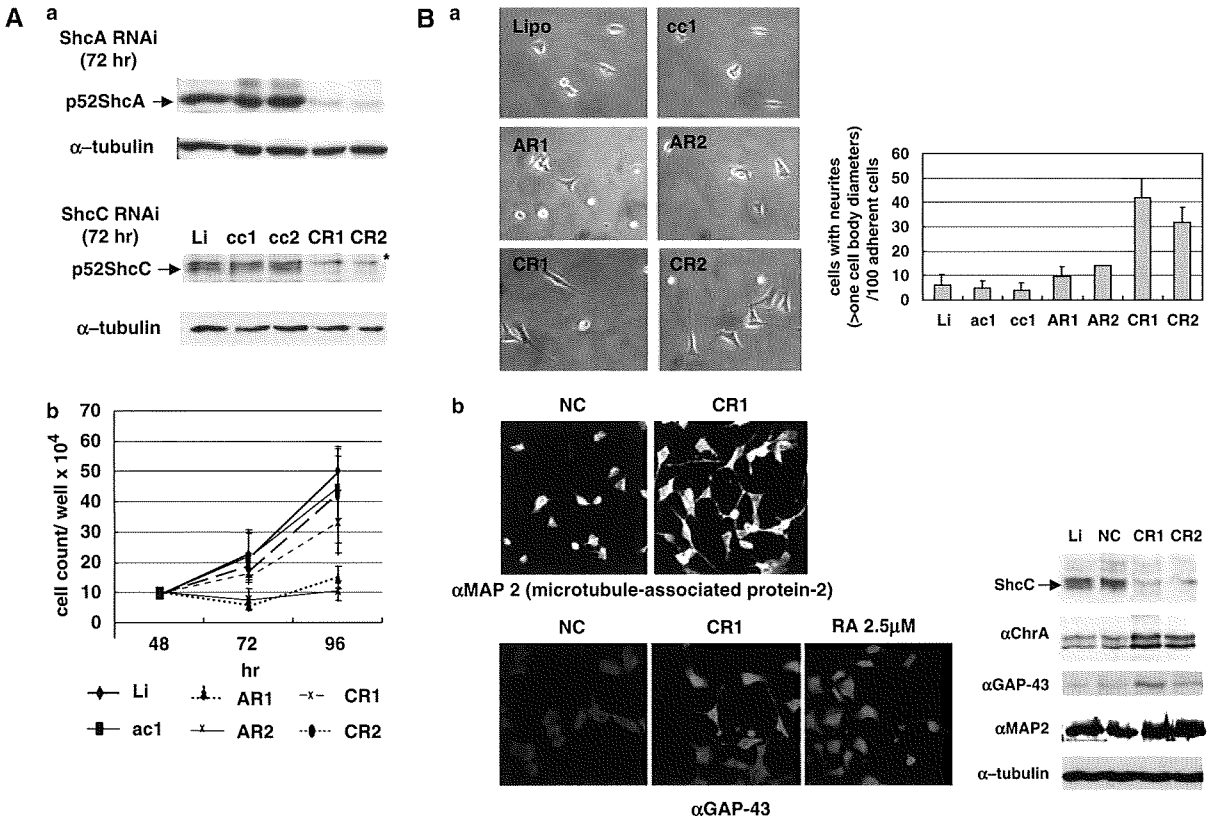

Figure 2 Biological effects of ShcC downregulation using small interfering RNA (siRNA) on TNB-1 cells. (**A**) (a) Expression of ShcC (lower panel) and ShcA (upper panel) was suppressed by RNA interference using specific siRNA oligonucleotides corresponding to ShcC and ShcA, respectively, then, detected by western analysis with each specific antibody. (b) Growth rate of siRNA-treated cells in tissue culture condition. TNB-1 cells 48 h after the transfection with ShcA/ShcC siRNA cultured by 30-mm dishes were counted at the indicated time points. The results represent the average values (± s.d.) of three replicated experiments. (**B**) Downregulation of ShcC induces neurite outgrowth and increases the expression of differentiation-related markers in TNB-1 cells. (a) Evaluation of neurite outgrowth of ShcA or ShcC-knockdown TNB-1 cells 72 h after siRNA treatment without any extracellular matrix (ECM) stimulation. (b) Expression of several molecules used as differentiation-related markers in ShcC-knockdown TNB-1 cells (left panel: immunostaining of neuritis as described in 'Materials and methods'; right panel: western analysis using indicated antibodies). As a positive control of differentiation, 2.5 μM retinoic acid (RA) was treated 24 h before analysis. AR1, AR2/CR1, CR2: two independent siRNA of ShcA /ShcC; Li: treated with only Lipofectamine 2000; ac1, ac2/cc1, cc2: control siRNA for ShcA /ShcC siRNA, respectively. NC: negative control for universal siRNA (as described in 'Materials and methods').

RNAi (miShcC-1, -2 and -3) were prepared by checking the level of ShcC protein along with clones of LacZ miR RNAi (miLacZ-1 and -2) as controls (Figure 6b). These clones with suppressed level of ShcC showed the same morphological features of neurite formation in tissue culture condition as observed in the cells transfected with ShcC siRNAs (data not shown). The volumes and weights of subcutaneous tumors in nude mice were measured at 6 weeks after injections of the cells and evaluated in at least 4 independent injections per clone. Control LacZ miR RNAi clones (miLacZ-1, miLacZ-2) developed large tumor masses *in vivo* (Figure 6c), whereas remarkable reduction of the size and weight of tumors (or almost disappearance of tumors in some cases) was observed by the stable suppression of ShcC expression. These tumors from ShcC miR RNAi clones showed marked increase in numbers of apoptotic cells compared with control tissues as shown by terminal transferase dUTP nick-end labeling (TUNEL) staining. On the other hand, staining by a proliferation marker, Ki-67 showed no significant difference among each tumor tissue (Figure 6d).

Discussion

It has already been shown that some signal pathways strongly affect tumor progression and treatment resistance (Schwab *et al*., 2003). Other than the Trk family, the PI3K/Akt pathway (Opel *et al*., 2007), Ret (Iwamoto *et al*., 1993; Marshall *et al*., 1997), hepatocyte growth factor/c-Met pathway (Hecht *et al*., 2004) were reported to be closely associated with several diagnostic profiles and biological characteristics of neuroblastoma cells.

This is the first study to show that the expression of ShcC protein, a member of the Shc family docking proteins, is significantly correlated with malignant phenotypes associated with advanced neuroblastoma. Expression of both p52 and p67 isoforms of ShcC,

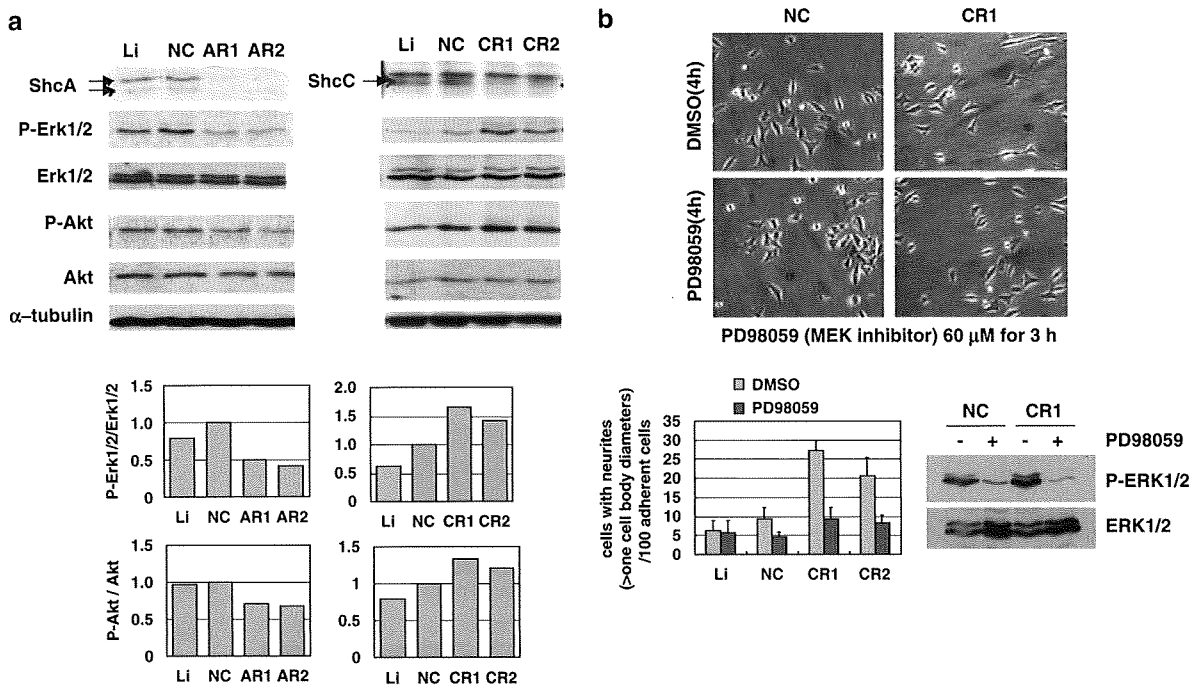

Figure 3 Persistent activation of extracellular signal-related kinase 1/2 (ERK1/2) in ShcC downregulation induces neurite outgrowth in TNB-1 cells. (**a**) Downregulation of ShcC positively affects the ERK1/2 and Akt pathway in TNB-1 cells. Activation of ERK1/2 and Akt in the cells treated with ShcA or ShcC siRNA were examined by western blotting. The levels of activation were quantified comparing to that of cells treated with control siRNA (NC). (**b**) Effect of MEK inhibitor on neurite outgrowth induced by ShcC RNAi in TNB-1 cells. The siRNA-transfected cells indicated were treated with dimethylsulphoxide (DMSO) or PD98059 and incubated for 3 h in the tissue culture condition, then counted for neurite-containing cells.

shows significant correlation with clinical stage and *MYCN* gene amplification whereas the expression of both isoforms of ShcA, p52 and p66, showed little association with those aspects. These results, in the protein level, give further evidence that ShcC is a factor which determines the prognosis of neuroblastoma, which was recently suggested by analysis of the mRNA expression of ShcC (Terui *et al.*, 2005).

The biological analysis of TNB-1 cells treated with ShcC-specific siRNAs provided evidence that ShcC protein expressed in the neuroblastoma cells is suppressing the differentiation of neuroblastoma cells. Neurite outgrowth of TNB-1 cells, induced by downregulation of ShcC was dependent on sustained activation of the MEK/ERK pathway. Sustained activation of the ERK pathway triggered by factors such as NGF is required for neuronal differentiation in some neuronal tumor cells such as PC12 cells (Qui and Green, 1992; Yaka *et al.*, 1998). The fact that constitutively activated Raf–ERK signaling induced neurite outgrowth in the same cell line (Supplementary Figure C), such as the RTK-related pathway might induce the ERK activation and cellular differentiation in TNB-1 cells, although NGF stimulation failed to induce neurite elongation of TNB-1 cells (data not shown).

Interestingly, elevation in the level of phosphorylated ShcA followed by activation of the ERK pathway by ShcA–Grb2 signals was observed in TNB1 when the ShcC protein expression was suppressed by RNAi. This activation of the ShcA–Grb2–ERK pathway caused by downregulation of ShcC may be due to a competitive effect between ShcC and ShcA for binding to certain RTKs. This possibility is supported by another experiment showing that both EGF-induced phosphorylation of ShcA and complex formation between ShcA and Grb2 in KU-YS cells are suppressed by the expression of ShcC in a dose-dependent manner. It was shown that the expression of the PTB domains of ShcC partially interfered with the binding of endogenous ShcA to activated EGFR in 293 cells (O'Bryan *et al.*, 1998). These data are consistent with our current findings described above. It is suspected that some types of differentiation signals mediated by ShcA are blocked by the overexpression of ShcC in some neuroblastoma cells such as TNB-1, and the suppression of ShcC protein by RNAi causes the ShcA-mediated differentiation of these cells.

Elevated level of ShcA phosphorylation and ERK activation induced by ShcC downregulation was more significant under the stimulation of collagen I than without any ECM stimulation. In addition, in suspending condition we could not detect any activation of ShcA nor ERK signal after ShcC downregulation (Supplementary Figure E). These results indicate that the difference between ShcA and ShcC might be in interaction with matrix-adhesion signals. ShcA is considered to be implicated in the adherent related pathway, phosphorylated by forming a complex with

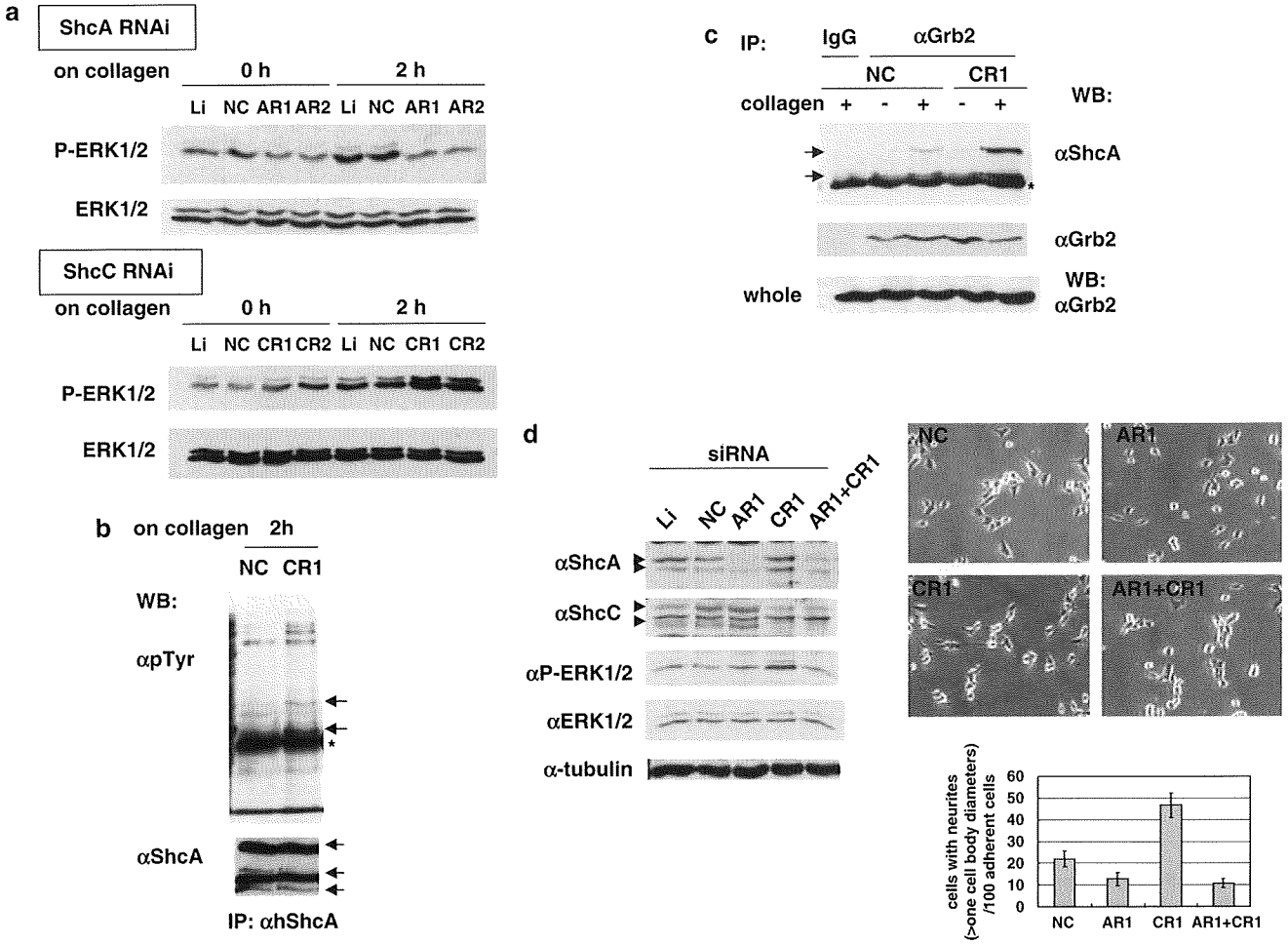

Figure 4 Elevation of extracellular signal-regulated kinase ()-activated level in ShcC-knockdown cells is increased by collagen stimulation by ShcA–Grb2 signaling. (**a**) Elevation of the ERK1/2-activated level due to ShcC downregulation is further increased 2 h after collagen stimulation. siRNAs of ShcA/ShcC-transfected TNB-1 cells (AR1, AR2/CR1, CR2, respectively) were incubated in the tissue culture condition for 70 h and stimulated by collagen type I. Duplicated cells were harvested 0 and 2 h after collagen stimulation (as described in 'Materials and methods'). (**b**) After collagen stimulation ShcA was phosphorylated more strongly in ShcC-knockdown cells than the control cells. Asterisks show heavy chains of immunoglobulin. (**c**) ShcA–Grb2 complex formation (upper panel) were increased by downregulation of ShcC. (**d**) The ShcA-knockdown effect on the neurite outgrowth in cells transfected with ShcC siRNA was evaluated by the same method performed in Figure 2Ba. The number of neurites observed in the cells transfected with both ShcA and ShcC siRNA was obviously decreased compared to cells transfected with only ShcC siRNA.

Fyn (Wary *et al*., 1998) through its proline-rich region that is not conserved in ShcC.

In tissue culture and in transgenic mice, signaling through Fyn has been closely associated with neurite extension and cell adhesion (Brouns *et al*., 2000, 2001). Berwanger *et al*. (2002) referred to the inverse correlation between the expression of Fyn and progression of neuroblastoma from 94 primary neuroblastoma specimens, showing that expressed Fyn-induced differentiation and growth arrest of neuroblastoma cell lines. Another report indicated that active Fyn kinase induces a lasting activation of the MAPK pathway through inhibition of MAPK phosphatase 1 (Wellbrock *et al*., 2002). We confirmed that neurite outgrowth of ShcC-knockdown TNB-1 cells was suppressed by Src family inhibitor, PP2 (Supplementary Figure H). These data suggest the possibility that Integrin–Fyn–ShcA signals could be closely associated with the differentiation of TNB-1 cells induced by ShcC downregulation along with the signals of RTK–ShcA/ShcC.

Noticeably, the interference of the ShcA-mediated signaling by ShcC protein is independent of tyrosine phosphorylation of ShcC. The function of the nonphosphorylated domain of ShcC such as SH2 might be also highlighted. As for the difference in the downstream signaling between ShcC and ShcA, little is known so far. Regarding to this point, Nakamura *et al*. (2002) indicated that inhibition of NGF-induced ERK activation by the expression of ShcC was due to the different Grb2-binding capacity between ShcA and ShcC in response to NGF. It was previously reported that ShcA preferentially binds to TrkA (Yamada *et al*., 2002), which is the key receptor against NGF due to neurite outgrowth with the sustained ERK phosphorylation,

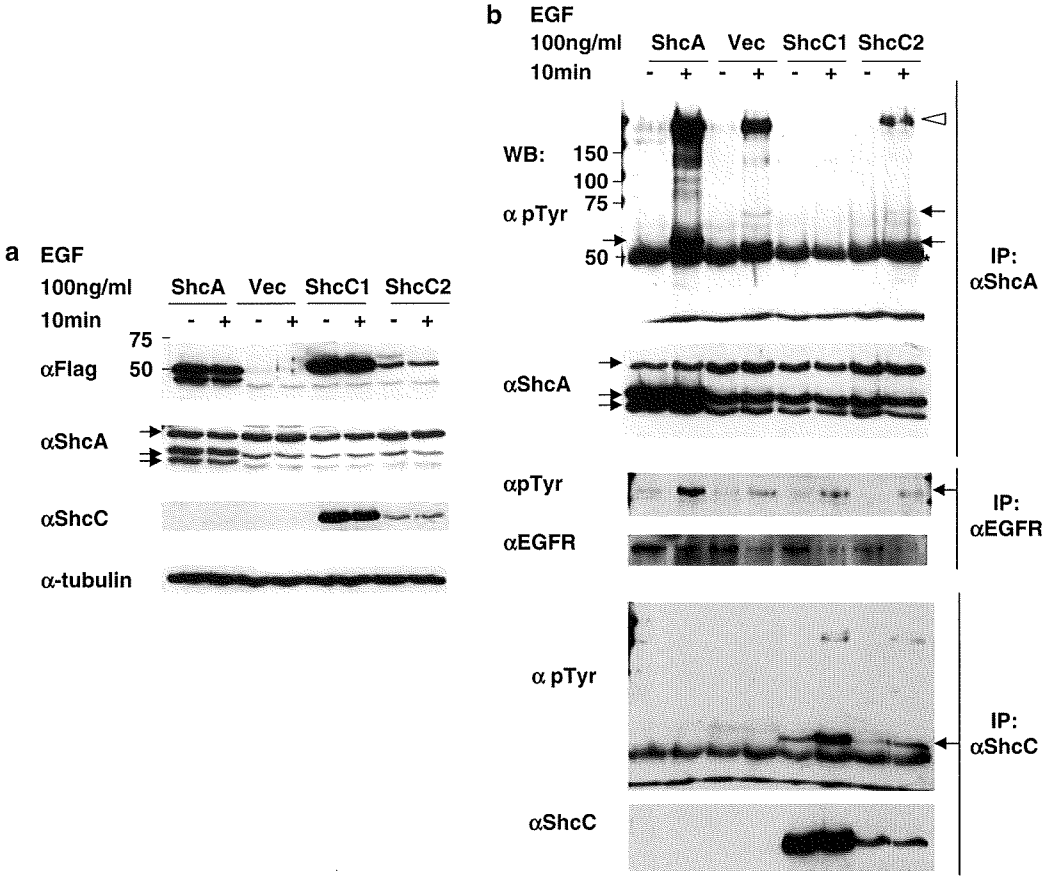

Figure 5 High expression of ShcC suppresses the phosphorylation of ShcA in KU-YS cells stimulated by epidermal growth factor (EGF). We generated stable clones of KU-YS cells expressing Flag-tagged ShcA and diverse levels of p52ShcC (ShcC1 and ShcC2) other than clones transfected with the control vector. (**a**) Each expression level was detected by western analysis. (**b**) Levels of expression and tyrosine phosphorylation of EGFR (middle panel), ShcA (upper panel) and ShcC (lower panel) were analysed by immunoprecipitation and immunoblotting using the antibodies indicated in figure in the KU-YS clone cells stimulated by EGF (as described in 'Materials and methods'). Asterisks show heavy chains of immunoglobulin.

whereas ShcC associated with TrkB rather than TrkA (O'Bryan *et al*., 1998; Liu and Meakin, 2002). In neuroblastoma, the function of signal pathways downstream of these two neurotrophin receptors might be quite different (Nakagawara *et al*., 1993), also suggesting the distinct function of downstream signal mediated by ShcC.

The effect of ShcC knockdown in *in vivo* tumorigenicity was quite remarkable comparing the effect in growth rate in tissue culture condition. We found that anchorage-independent growth in cells was also dramatically decreased by knockdown of ShcC as shown by soft agar assay (Figure 6a). Furthermore, the proportion of apoptotic cells in the nude mouse tumors generated from neuroblastoma cells *in vivo* was remarkably increased by the knockdown of ShcC. In recent study, Magrassi *et al*. (2005) showed that ShcC positively effects on cell survival by PI3K–AKT pathway in glioma cells using dominant negative form of ShcC. Theses data indicate that ShcC has additional function in the protection from some types of apoptosis in addition to the induction of differentiation of cells.

It was indicated that ShcC might have a potent function for tumor progression in neuroblastoma by suppressing the differentiation and by promoting the anchorage-independent growth in the majority of neuroblastoma cells which has high expression of ShcC protein. From these points of view, we suggest that ShcC is a potent tool for predicting the phenotype of neuroblastoma and is also a good candidate for therapeutic targets of advanced neuroblastoma.

Materials and methods

Cell culture and tissue samples

DLD-1 cells and all cell lines of neuroblastomas in this study were prepared as described in the previous report (Miyake *et al*., 2002). These cells were cultured in an RPMI 1640 medium with 10% fetal calf serum (FCS) (Sigma, St Louis, MO, USA) at 37 °C in an atmosphere containing 5% CO_2.

Anonymous 46 frozen neuroblastoma tissues were used in this study. The samples were divided into three subsets using Brodeur's classification; type I (stage 1, 2 or 4S; a single copy of *MYCN*), type II (stage 3 or 4; a single copy of *MYCN*) and type III (all stages; amplification of *MYCN*) (Brodeur and Nakagawara, 1992; Ohira *et al*., 2003). A total of 15 samples belonged to type I, 18 samples to type II and 13 samples to type III. Staging classification was according to the

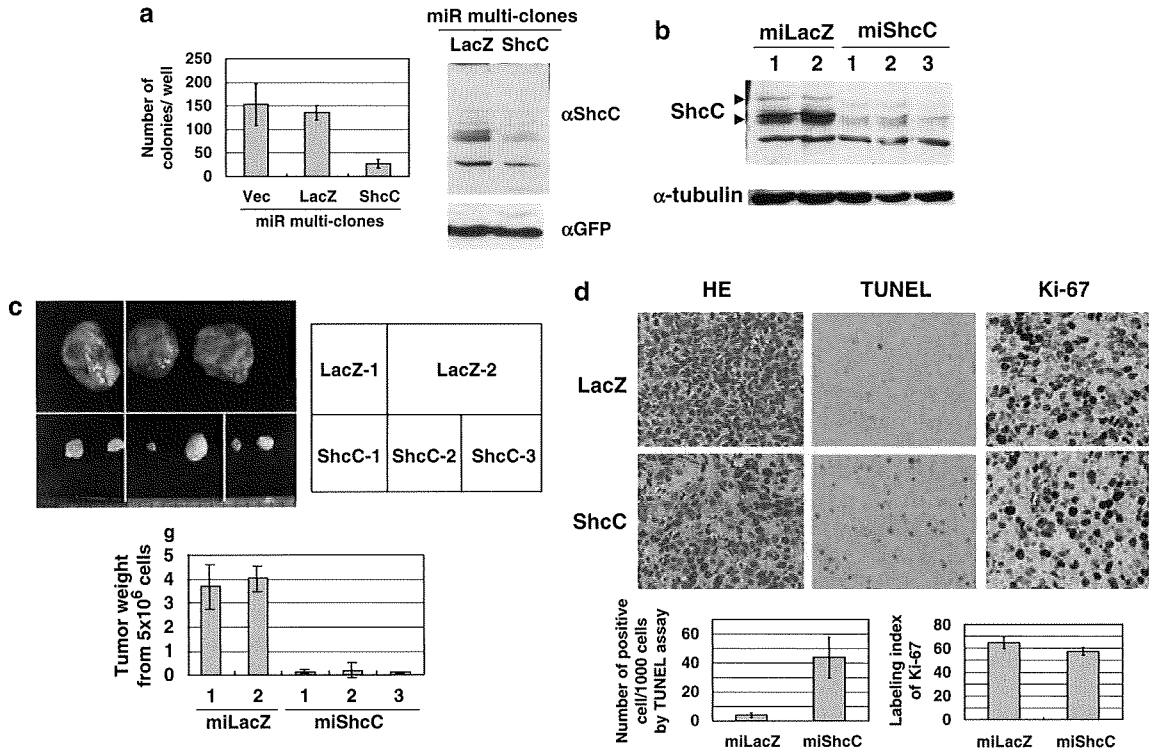

Figure 6 ShcC downregulation negatively affects tumorigenicity *in vivo*. (**a**) Cells transfected with the miR RNAi vector for ShcC (miShcC) and LacZ (miLacZ) that also contains an EmGFP coding sequence for co-cistronic expression with the pre-miRNA were cultured in medium containing blasticidin (Invivogen) for only 1 week, and then mixed. Multiclone cells for LacZ and ShcC were analysed for the ability of anchorage-independent growth using soft agar assay by 1×10^4 cells per a well of six-well plate for 3 weeks (as described in previous report: Miyake *et al*., 2005). The results represent the average value (± s.d.) of three replicated experiments. (**b**) Expression levels of ShcC in clones of TNB-1 cells stably transfected with miR RNAi expression vector for LacZ (miLacZ-1 and miLacZ-2) and ShcC (miShcC-1, -2 and -3) were detected by western analysis using αhShcC (as described in 'Materials and methods'). (**c**) Nude mouse tumors derived from two clones of LacZ miR RNAi and three clones of ShcC. Upper panel: Photographs of tumors from nude mice at 6 weeks after subcutaneous injections of 5×10^6 cloned cells (bar: 20 mm); lower panel: ability of *in vivo* tumorigenicity is shown by average weight (±) of four tumor derived from each clone. (**d**) ShcC-knockdown cells show tendency to apoptosis *in vivo*. Upper panel: Photographs of a cross-section of each tumor tissues from miLacZ-1 and miShcC-2 using microscope at a magnification of × 400, that were stained with hematoxylin and eosin (HE), diaminobenzidine (DAB) by terminal transferase dUTP nick-end labeling (TUNEL) assay and anti-Ki-67 antibody (bar: 25 μm); lower panel: the tendency to apoptosis was defined as the number of positive stained cells per 1000 tumor cells in TUNEL assay and the proliferating activity was indicated as the labeling index of Ki-67 by counting 1000 tumor cells. The data show the average scores ± s.d. of positive cells in three different areas of each slide. Staining of each sample was owing to the procedure by SRL Inc.

International Neuroblastoma Staging System and *N-Myc* amplification (> 10 copy) accepted as a poor prognostic risk factor was checked before clinical intervention.

Reagents

The polyclonal antibodies against the CH1 domain of human ShcC (amino acid 225–324):αhShcC were generated by the same method as described previously (Miyake *et al*., 2002). Polyclonal antibodies of human ShcA:αhShcA were prepared as described in previous reports (Miyake *et al*., 2002).

Other antibodies were purchased as follows: antiphosphotyrosine antibody (4G10) (Upstate Biotechnology Inc., Charlottesville, VA, USA), anti-ShcA/ShcC monoclonal antibodies: αShcA/αShcC (BD Transduction Laboratories, San Diego, CA, USA), anti-α-tubulin antibody (Zymed Laboratories, San Francisco, CA, USA), anti-p44/42 MAPK (ERK1/2), anti-phospho-p44/42 MAPK (P-ERK1/2), anti-Akt, and anti-phospho-Akt (Ser473) (P-Akt) antibodies (Cell Signaling, Danvers, MA, USA), anti-chromogranin A (ChrA) antibody (Santa Cruz Biotechnology, Santa Cruz, CA, USA), anti-GAP43 antibody (Zymed Laboratories), anti-MAP2 antibody (Santa Cruz Biotechnology), anti-c-Src antibody (Upstate Biotechnology Inc.), anti-phospho-Src family antibody (Tyr416) (Cell Signaling), anti-Grb2 antibody (BD Transduction Laboratories), anti-T7tag antibody (Novagen, San Diego, CA, USA) and anti-Flag M2 antibody (Sigma). As secondary antibodies, horseradish peroxidase-conjugated anti-rabbit and anti-mouse IgGs (GE Healthcare, Buckinghamshire, UK) were used. All inhibitors used in this study (PD98059, LY294002, PP2 and PP3) were purchased from Calbiochem, San Diego, CA, USA.

Cell stimulation, immunoprecipitation and immunoblotting

Cell stimulation analysis with EGF (Wako) was performed as described (Miyake *et al*., 2002). The cells were starved for 24 h and treated for 5 min with EGF (100 ng/ml). As for stimulation with collagen type I, cultured cells with or without serum for 24 h were detached from culture dishes by pipette treatment and after the suspending condition for 30 min, seeded onto a collagen type I-coated dish (Iwaki, Tokyo, Japan). Cells were harvested after 2 h using PLC lysis buffer. Control cells were harvested before the attachment on the collagen I-coated

surface. The immunoprecipitation and western analysis were performed using the procedure described in a previous report (Miyake *et al.*, 2002).

Quantification and statistical analysis of expression levels of ShcC/ShcA

The intensity of each band obtained by western analysis was measured using a molecular imager (GS-800; Bio-Rad, Hercules, CA, USA) and standardized according to control signals, such as the bands of TNB-1 and α-tubulin.

t-Test performed by Excel was used to evaluate the significance of the two groups quantified expression levels of indicated molecules.

Knockdown of ShcA/ShcC by RNA interference

For siRNAs, Stealth RNA duplex oligoribonucleotides (Invitrogen, Carlsbad, CA, USA) was used to knockdown ShcC/ShcA protein. The following two 25-mer oligonucleotide pairs for each molecule were available. As for ShcC, CR1: 5′-GCUGGCCAAAGCGCUCUAUGACAAU-3′ (nucleotides 141–165), CR2: 5′-CCAAGAUCUUUGUGGCGCACA GCAA-3′ (nucleotides 2447–2471). As negative controls for each oligonucleotide pair, cc1: GGCUCCAGAACGGCCUUAGU AACAU-3′, cc2: GGAAACCGACAACUACGAUGUCAAU, respectively. As for ShcA, AR1: 5′-GGAGUAACCUGAA AUUUGCUGGAAU-3′ (nucleotides 335–359). AR2: 5′-GCCU UCGAGUUGCGCUUCAAACAAU-3′ (nucleotides 689–611). As a negative control for each, ac1: GGAAACCGUAAUAUU CGGUGUGAA, ac2: 5′-UGCCGCGAUUCGCGUUACAAC UUAAU, respectively. As the other negative control for universal siRNA, Stealth RNAi Negative Control Duplexes (Medium GC Duplex) (Invitrogen) was used (NC). Cells were transfected with siRNA using Lipofectamine 2000 (Invitrogen) according to the manufacturer's instructions. Cells (5×10^5 per well of a six-well plate) in suspending condition were transfected twice at 24 h interval (5 μl of 20 μM siRNA each) and analysed 48 h after second transfection.

A system stably expressing miRNA was generated using the BLOCK-iT Pol II miR RNAi Expression Vector Kit with EmGFP (Invitrogen) according to the manufacturer's instructions. In the generation of the miR RNAi vector for humans, ShcC was chosen as the target sequence, using the top/bottom oligo sequence: 5′-TGCTGCTTGGAGGCTTTCTCTTCTT GGTTTTGGCCACTGACTGACCAAGAAGAAAGCCTC CAAG-3′/5′-CCTGCTTGGAGGCTTTCTTCTTGGTCAGTC AGTGGCCAAAACCAAGAAGAGAAAGCCTCCAAGC-3′. Cells stably expressing the miR RNAi vector for ShcC (miShcC) and LacZ (miLacZ), that were also expressing green fluorescent protein were established and cultured in medium containing blasticidin (InvivoGen, San Diego, CA, USA) at a concentration of 15 μg/ml for 3 weeks. Three clones expressing the ShcC RNAi vector were selected by significant suppression of the ShcC protein (< 10%), and two clones from the control LacZ vector were also selected. Cells transfected with miR-negative control plasmid (one of kit components) were used as other control cells (Vec).

Generation of KU-YS cells stably expressing ShcA/ShcC

The full-length human ShcA cDNA for transfection was donated by Dr N Goto. ShcA and ShcC cDNAs were inserted with C-terminal Flag epitope tag into a mammalian expression vector pcDNA3.1A. All parts amplified by PCR were verified by sequencing. The stable expression of the full-length of ShcA and full-length of ShcC in KU-YS cells were obtained by transfection using transfection reagent Lipofectamine 2000 (Invitrogen) according to the manufacturer's instructions. The KU-YS cells transfected with pcDNA3.1 vector (mock) were used as a control. Then, cells were selected according to the method described previously and the expression level of each independent clone was evaluated by immunoblotting analysis.

Acknowledgements

This work was supported by a Grant-in-Aid from the Ministry of Health, Labor and Welfare of Japan for the third-term Comprehensive 10-year Strategy for Cancer Control.

References

Berwanger B, Hartmann O, Bergmann E, Bernard S, Nielsen D, Krause M *et al.* (2002). Loss of a FYN-regulated differentiation and growth arrest pathway in advanced stage neuroblastoma. *Cancer Cell* **2**: 377–386.

Brodeur GM, Nakagawara A. (1992). Molecular basis of clinical heterogeneity in neuroblastoma. *Am J Pediatr Hematol Oncol* **14**: 111–116.

Brouns MR, Matheson SF, Hu KQ, Delalle I, Caviness VS, Silver J *et al.* (2000). The adhesion signaling molecule p190 RhoGAP is required for morphogenetic processes in neural development. *Development* **127**: 4891–4903.

Brouns MR, Matheson SF, Settleman J. (2001). p190 RhoGAP is the principal Src substrate in brain and regulates axon outgrowth, guidance and fasciculation. *Nat Cell Biol* **3**: 361–367.

Dhillon AS, Meikle S, Peyssonnaux C, Grindlay J, Kaiser C, Steen H *et al.* (2003). A Raf-1 mutant that dissociates MEK/extracellular signal-regulated kinase activation from malignant transformation and differentiation but not proliferation. *Mol Cell Biol* **23**: 1983–1993.

Giudici AM, Sher E, Pelagi M, Clementi F, Zanini A. (1992). Immunolocalization of secretogranin II, chromogranin A, and chromogranin B in differentiating human neuroblastoma cells. *Eur J Cell Biol* **58**: 383–389.

Hecht M, Papoutsi M, Tran HD, Wilting J, Schweigerer L. (2004). Hepatocyte growth factor/c-Met signaling promotes the progression of experimental human neuroblastomas. *Cancer Res* **64**: 6109–6118.

Hecker TP, Grammer JR, Gillespie GY, Stewart Jr J, Gladson CL. (2002). Focal adhesion kinase enhances signaling through the Shc/extracellular signal-regulated kinase pathway in anaplastic astrocytoma tumor biopsy samples. *Cancer Res* **62**: 2699–2707.

Hinsby AM, Lundfald L, Ditlevsen DK, Korshunova I, Juhl L, Meakin SO *et al.* (2004). ShcA regulates neurite outgrowth stimulated by neural cell adhesion molecule but not by fibroblast growth factor 2: evidence for a distinct fibroblast growth factor receptor response to neural cell adhesion molecule activation. *J Neurochem* **91**: 694–703.

Iwamoto T, Taniguchi M, Wajjwalku W, Nakashima I, Takahashi M. (1993). Neuroblastoma in a transgenic mouse carrying a metallothionein/ret fusion gene. *Br J Cancer* **67**: 504–507.

Leevers SJ, Paterson HF, Marshall CJ. (1994). Requirement for Ras in Raf activation is overcome by targeting Raf to the plasma membrane. *Nature* **369**: 411–414.

Liu HY, Meakin SO. (2002). ShcB and ShcC activation by the Trk family of receptor tyrosine kinases. *J Biol Chem* **277**: 26046–26056.

Magrassi L, Conti L, Lanterna A, Zuccato C, Marchionni M, Cassini P *et al.* (2005). Shc3 affects human high-grade astrocytomas survival. *Oncogene* **24**: 5198–5206.

Marshall GM, Peaston AE, Hocker JE, Smith SA, Hansford LM, Tobias V *et al.* (1997). Expression of multiple endocrine neoplasia 2B RET in neuroblastoma cells alters cell adhesion *in vitro*, enhances

metastatic behavior *in vivo*, and activates Jun kinase. *Cancer Res* **57**: 5399–5405.

Miyake I, Hakomori Y, Misu Y, Nakadate H, Matsuura N, Sakamoto M *et al.* (2005). Domain-specific function of ShcC docking protein in neuroblastoma cells. *Oncogene* **24**: 3206–3215.

Miyake I, Hakomori Y, Shinohara A, Gamou T, Saito M, Iwamatsu A *et al.* (2002). Activation of anaplastic lymphoma kinase is responsible for hyperphosphorylation of ShcC in neuroblastoma cell lines. *Oncogene* **21**: 5823–5834.

Moro L, Venturino M, Bozzo C, Silengo L, Altruda F, Beguinot L *et al.* (1998). Integrins induce activation of EGF receptor: role in MAP kinase induction and adhesion-dependent cell survival. *EMBO J* **17**: 6622–6632.

Nakagawara A, Arima-Nakagawara M, Scavarda NJ, Azar CG, Cantor AB, Brodeur GM. (1993). Association between high levels of expression of the TRK gene and favorable outcome in human neuroblastoma. *N Engl J Med* **328**: 847–854.

Nakagawara A, Brodeur GM. (1997). Role of neurotrophins and their receptors in human neuroblastomas: a primary culture study. *Eur J Cancer* **33**: 2050–2053.

Nakamura T, Komiya M, Gotoh N, Koizumi S, Shibuya M, Mori N. (2002). Discrimination between phosphotyrosine-mediated signaling properties of conventional and neuronal Shc adapter molecules. *Oncogene* **21**: 22–31.

Nakamura T, Muraoka S, Sanokawa R, Mori N. (1998). N-Shc and Sck, two neuronally expressed Shc adapter homologs. Their differential regional expression in the brain and roles in neurotrophin and Src signaling. *J Biol Chem* **273**: 6960–6967.

Nakamura T, Sanokawa R, Sasaki Y, Ayusawa D, Oishi M, Mori N. (1996). N-Shc: a neural-specific adapter molecule that mediates signaling from neurotrophin/Trk to Ras/MAPK pathway. *Oncogene* **13**: 1111–1121.

O'Bryan JP, Lambert QT, Der CJ. (1998). The src homology 2 and phosphotyrosine binding domains of the ShcC adaptor protein function as inhibitors of mitogenic signaling by the epidermal growth factor receptor. *J Biol Chem* **273**: 20431–20437.

O'Bryan JP, Songyang Z, Cantley L, Der CJ, Pawson T. (1996). A mammalian adaptor protein with conserved Src homology 2 and phosphotyrosine-binding domains is related to Shc and is specifically expressed in the brain. *Proc Natl Acad Sci USA* **93**: 2729–2734.

Ohira M, Morohashi A, Inuzuka H, Shishikura T, Kawamoto T, Kageyama H *et al.* (2003). Expression profiling and characterization of 4200 genes cloned from primary neuroblastomas: identification of 305 genes differentially expressed between favorable and unfavorable subsets. *Oncogene* **22**: 5525–5536.

Opel D, Poremba C, Simon T, Debatin KM, Fulda S. (2007). Activation of Akt predicts poor outcome in neuroblastoma. *Cancer Res* **67**: 735–745.

Osajima-Hakomori Y, Miyake I, Ohira M, Nakagawara A, Nakagawa A, Sakai R. (2005). Biological role of anaplastic lymphoma kinase in neuroblastoma. *Am J Pathol* **167**: 213–222.

Pelicci G, Dente L, De Giuseppe A, Verducci-Galletti B, Giuli S, Mele S *et al.* (1996). A family of Shc related proteins with conserved PTB, CH1 and SH2 regions. *Oncogene* **13**: 633–641.

Qui MS, Green SH. (1992). PC12 cell neuronal differentiation is associated with prolonged p21ras activity and consequent prolonged ERK activity. *Neuron* **9**: 705–717.

Ravichandran KS. (2001). Signaling via Shc family adapter proteins. *Oncogene* **20**: 6322–6330.

Sakai R, Henderson JT, O'Bryan JP, Elia AJ, Saxton TM, Pawson T. (2000). The mammalian ShcB and ShcC phosphotyrosine docking proteins function in the maturation of sensory and sympathetic neurons. *Neuron* **28**: 819–833.

Schwab M, Westermann F, Hero B, Berthold F. (2003). Neuroblastoma: biology and molecular and chromosomal pathology. *Lancet Oncol* **4**: 472–480.

Stokoe D, Macdonald SG, Cadwallader K, Symons M, Hancock JF. (1994). Activation of Raf as a result of recruitment to the plasma membrane. *Science* **264**: 1463–1467.

Terui E, Matsunaga T, Yoshida H, Kouchi K, Kuroda H, Hishiki T *et al.* (2005). Shc family expression in neuroblastoma: high expression of shcC is associated with a poor prognosis in advanced neuroblastoma. *Clin Cancer Res* **11**: 3280–3287.

Wary KK, Mainiero F, Isakoff SJ, Marcantonio EE, Giancotti FG. (1996). The adaptor protein Shc couples a class of integrins to the control of cell cycle progression. *Cell* **87**: 733–743.

Wary KK, Mariotti A, Zurzolo C, Giancotti FG. (1998). A requirement for caveolin-1 and associated kinase Fyn in integrin signaling and anchorage-dependent cell growth. *Cell* **94**: 625–634.

Wellbrock C, Weisser C, Geissinger E, Troppmair J, Schartl M. (2002). Activation of p59(Fyn) leads to melanocyte dedifferentiation by influencing MKP-1-regulated mitogen-activated protein kinase signaling. *J Biol Chem* **277**: 6443–6454.

Yaka R, Gamliel A, Gurwitz D, Stein R. (1998). NGF induces transient but not sustained activation of ERK in PC12 mutant cells incapable of differentiating. *J Cell Biochem* **70**: 425–432.

Yamada M, Numakawa T, Koshimizu H, Tanabe K, Wada K, Koizumi S *et al.* (2002). Distinct usages of phospholipase C gamma and Shc in intracellular signaling stimulated by neurotrophins. *Brain Res* **955**: 183–190.

Supplementary Information accompanies the paper on the Oncogene website (http://www.nature.com/onc)

A preoperative evaluation for neo-infantile liver tumors using a three-dimensional reconstruction of multidetector row CT

YOSHIAKI KINOSHITA[1], RYOTA SOUZAKI[1], TATSURO TAJIRI[1], SATOSHI IEIRI[1,2], MAKOTO HASHIZUME[2] and TOMOAKI TAGUCHI[1]

[1]Department of Pediatric Surgery, Graduate School of Medical Sciences, Kyushu University, [2]Center for the Integration of Advanced Medicine and Innovative Technology, Kyushu University Hospital, Fukuoka 812-8582, Japan

Received September 5, 2008; Accepted December 9, 2008

DOI: 10.3892/or_00000298

Abstract. Multidetector row CT (MDCT), which has been used extensively in adult patients, has also recently been used for the evaluation of children. As pediatric surgeons, we preoperatively examined 10 cases of liver tumors by MDCT and performed three-dimensional reconstruction and a volumetric analysis. Instead of angiography, which requires general anesthesia in children, this method can provide a fine image of the anatomy between the tumor and the vessels, as well as identify the presence of any anomalous vascular branches. It also makes it possible to calculate the residual liver volume for the proposed operation and to determine the optimal cut line. However, there are still certain problems associated with pediatric cases, including the determination of the appropriate volume of contrast medium, the occurrence of allergic reactions to the contrast medium, and the timing of enhancement. The resolution of the specific problems in the pediatric application of MDCT, and the development of a more effective procedure is thus required.

Introduction

Currently multidetector row CT (MDCT) has made it possible to obtain more valuable information than was previously possible with conventional CT. The MDCT is superior in spatial and temporal resolutions. In adult cases, the MDCT has been frequently applied as a diagnostic tool for tumors. In pediatric cases, however, some such problems as the necessity to use anesthesia, difficulty of respiratory restriction, determining the adequate volume of contrast medium, and the estimated irradiation have been recognized, the application of MDCT procedures in the pediatric population has therefore been limited. The development of the multidetector (16 or 64 slice spirals) has solved some of these problems. This study presents 10 cases of pediatric liver tumors, which were evaluated by MDCT using three-dimensional reconstruction and volumetry.

Correspondence to: Dr Yoshiaki Kinoshita, Department of Pediatric Surgery, Graduate School of Medical Sciences, Kyushu University, 3-1-1, Maidashi, Higashi-ku, Fukuoka 812-8582, Japan
E-mail: kinoppy@pedsurg.med.kyushu-u.ac.jp

Key words: multidetector row CT, liver tumor, angiography, volumetry, child

Patients and methods

In our department, 10 cases of neo-infantile liver tumors were admitted from 2003 to 2007. Each case was examined preoperatively by MDCT. The clinical data of the patients are summarized in Table I. Regarding the age, 1 case was a neonate, 6 cases were infants younger than 1 year, and 3 cases were infants older than 1 year. Histologically, 7 cases had hepatoblastomas, 2 cases had infantile hemangioendotheliomas, and the remaining case was a malignant rhabdoid tumor. Six cases were treated by preoperative chemotherapy with cisplatin (CDDP) and pirarubicin (THP-adriamycin). Preoperative angiography with a transcatheter arterial chemoembolization (TACE) was performed for 5 cases, which showed insufficiency only for the preoperative systemic chemotherapy.

The scanning was performed by an MDCT with 64 detectors. As the contrast medium, iopamidole (300 mg/ml) was administered intravenously for 20 sec with a dose of 2 ml/kg. The condition of collimation was 1 or 2 mm and the herical pitch was 5.5. The arterial phase, equilibrium phase, and portal venous phase were captured in that order.

Triclofossodium syrup or pentobarbital suppositories were routinely used as sedative agents. Intravenous ketamine instillation was added in some cases. All cases were well sedated and high quality images were acquired under spontaneous respiration.

The images from MDCT were transferred to a 3D workstation (Virtual Place Advance, AZE) and then were analyzed. By this method, the feeding vessels and accessory or aberrant vessels were evaluated. In addition, the vessel architecture, including the arterial system and portal venous system were independently demonstrated and reconstructed as each phase analysis. As a volumetric 3D-rendered analysis, the standard liver volume and residual liver volume for several patterns of proposed operation were calculated (1). The standard liver volume (SLV) was also calculated by the Urata equation:

Table I. Clinical data of each case.

Case	Age	Gender	Histology	Location of tumor	Preoperative chemotherapy	Angio + TACE
1	14 days	F	HB	Rt. lobe	ND	ND
2	3 months	F	HB	S3, 4, 5, 6	Done	Done
3	4 months	M	HB	Lt. lobe	Done	Done
4	8 months	F	HB	Lt. lobe	Done	Done
5	1 year	F	HB	Rt. lobe	Done	ND
6	1 year	M	HB	Rt. lobe	ND	ND
7	3 years	M	HB	Rt. lobe	Done	Done
8	5 months	M	MRT	Rt. lobe, S4	Done	Done
9	1 month	M	HET	S3	ND	ND
10	1 month	F	HET	Bil. lobe	ND	ND

HB, hepatoblastoma; MRT, malignant rhabdoid tumor; HET, hemangioendothelioma; ND, not done; TACE, transcatheter arterial chemoembolization.

Table II. Abnormal vessels demonstration and volumetry analysis for each case.

Case	Abnormal vessels demonstration by MDCT	Proposed operation	SLV (ml)	RLV (ml)	RLV (%)
1	None	Rt. lobectomy	114.1	67.4	59.0
2	SMA→RHA, LGA→LHA	Central bisegmentectomy	497.2	294.5	59.2
3	None	Lt. lobectomy	267.9	213.1	79.0
4	None	Extended lt.lobectomy	296.5	160.0	54.0
5	Lt. IVC	Rt. lobectomy	284.1	190.4	67.0
6	None	Rt. lobectomy	109.2	68.1	62.4
7	None	Rt. lobectomy	398.6	259.1	65.0
8	CA→MHA, LGA→LHA	Extended rt. lobectomy	233.0	95.3	40.9
9	None	Tumor extirpation	176.8	161.3	91.2
10	None	Biopsy	NA	NA	NA

SMA, superior mesenteric artery; RHA, right hepatic artery; LGA, left gastric artery; LHA, left hepatic artery; CA, celiac artery; MHA, middle hepatic artery; SLV, standard liver volume; RLV, residual liver volume; NA, not analyzed.

Table III. Advantages for each case obtained by MDCT reconstruction.

Case	Detection of abnormal vessels or feeding arteries	No need for angiography	Advantage by simultaneous visualization of each phase	Advantage by simulation of proposed operation
1		○	○	
2	○		○	○
3			○	
4			○	○
5	○	○	○	
6		○	○	
7			○	
8	○		○	○
9	○	○	○	
10	○	○	○	

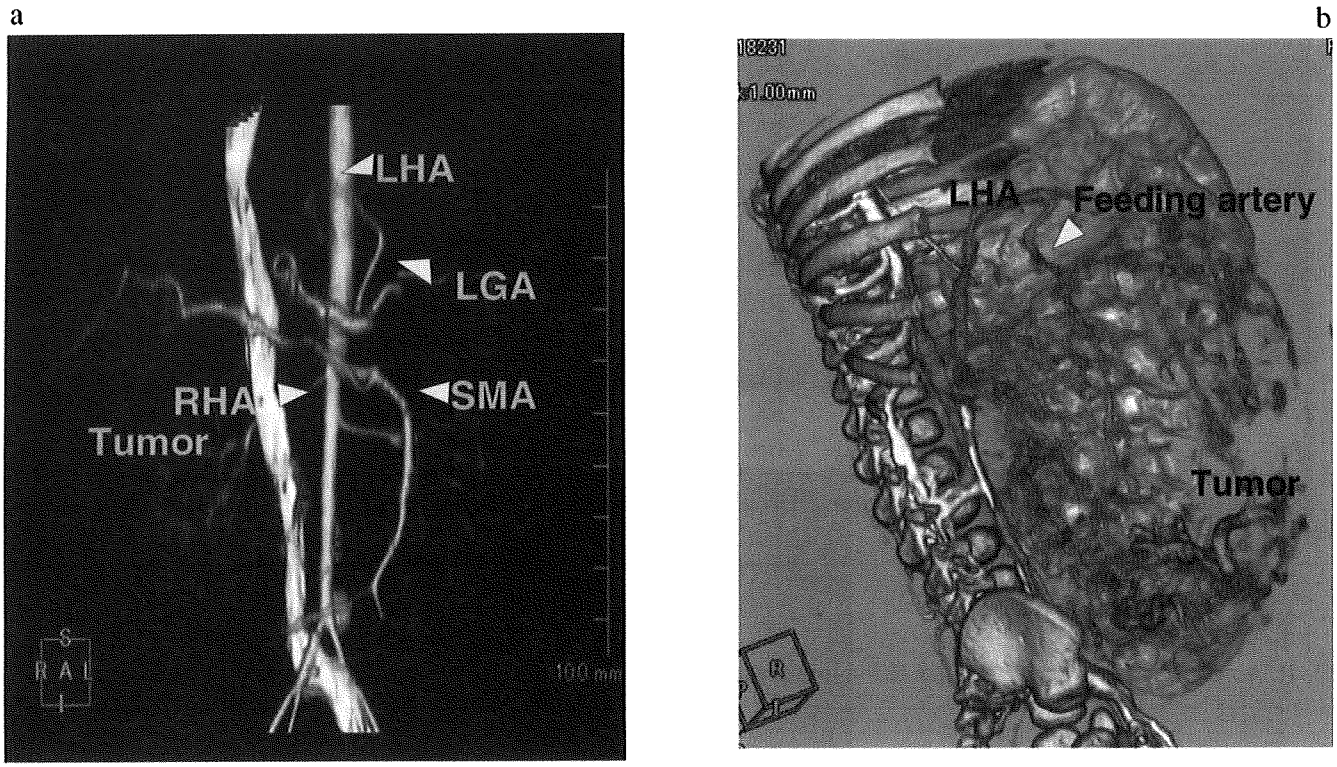

Figure 1. Detection of anomalous vessels and feeding vessels. (a) Case 6 (hepatoblastoma). The left hepatic artery (LHA) was observed to branch from the left gastric artery (LGA). The right hepatic artery (RHA) branched from the superior mesenteric artery (SMA). (b) Case 9 (hemangioendothelioma). The tumor feeding artery from the left hepatic artery (LHA) is detected by 3-D reconstruction images.

SLV (ml) = 706.2 x body surface area (m^2) (2). These reconstruction and volumetric analyses were performed by ourselves, namely by the 'pediatric surgeons'.

Results

Detection of anomalous vessels and feeding vessels. Abnormal vessels were detected in 3 cases (cases 2, 5, 8) (Table II). In case 2, the reconstructed image detected anomalous branching in the left hepatic artery (LHA) arising from left gastric artery (LGA) and the right hepatic artery (RHA) arising from the superior mesenteric artery (SMA) (Fig. 1a). In the same way, anomalous branching vessels were detected in cases 5 and 8. Furthermore, this procedure also clearly demonstrated the feeding vessels of huge tumors in cases 9 and 10. In case 9, the huge tumor was fed by a branching artery from the LHA (Fig. 1b). Those images were never inferior to those obtained from angiography and were very informative for the operation. In this manner, abnormal vessels or feeding arteries were detected in 5 cases. Since this vascular informations obtained by the reconstruction of the MDCT images was sufficient, conventional angiography was unnecessary for these 5 cases (Table III).

Each phase analysis. As shown by the images of case 5 (a one-year-old girl with a hepatoblastoma in the right lobe) (Fig. 2a), each contrast phase, arterial phase (Fig. 2b), equilibrium phase (Fig. 2c), and portal venous phase (Fig. 2d) were independently extracted or combined as three-dimensional images, respectively (Fig. 2e). By this method, the precise anatomical association between the tumor and vessels could be clearly demonstrated simultaneously. Since the simultaneous evaluation of identical images is impossible by conventional CT, this advantage was thus considered to be remarkable in all cases (Table III).

Volumetry analysis. The residual liver volume was calculated by a volumetric analysis for all cases (Table II). Since the whole liver was occupied by the tumor in case 10, the proposed operation was a biopsy. In the other 6 cases (cases 1, 3, 5, 6, 7, 9), the residual liver volume was calculated as >50% in the initially proposed operative procedure. Therefore, an optimal cut line was defined by this volumetric analysis. However, in the remaining cases (cases 2, 4, 8), the cut lines were variously simulated in several ways, because a sufficient residual liver volume was not expected by means of an extended operation. For example, in case 2, the tumor occupied the central area of the liver and it was attached to the portal vein (Fig. 3a); therefore, various operative procedures were simulated. The standard liver volume of the patient was calculated at 497.2 ml. If the patients would have undergone a left trisegmentectomy, then the residual liver volume would only have been 28.3% of the standard liver volume (Fig. 3b). On the other hand, if a central bisegmentectomy could be performed, then the residual liver volume was estimated to be 59.2% of the standard liver volume (Fig. 3c). Therefore,

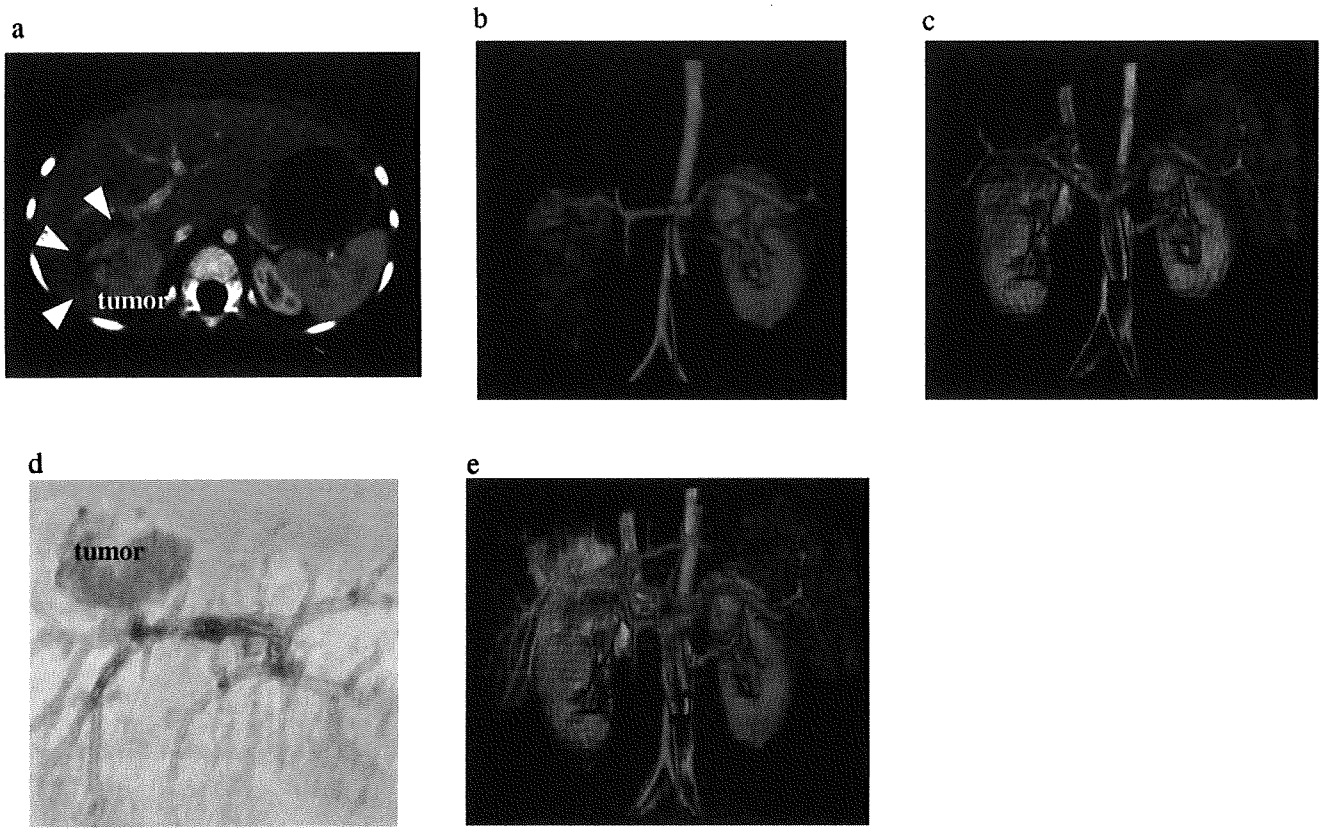

Figure 2. Each phase analysis (Case 5). (a) A 2-D image from a conventional CT. (b) A reconstructed image of the arterial phase. (c) A reconstructed image of the equilibrium phase. (d) A reconstructed image of the portal venous phase. (e) A reconstructed image of the combined multiphase images.

the central bisegmentectomy was selected for the preservation of postoperative liver function. Using these analyses, the most appropriate operation was performed in all cases.

Discussion

MDCT has multiple detectors along the body axis and simultaneouly provides a vast amount of information during one rotation of the X-ray tube. In comparison to the conventional helical CT, MDCT is superior in both temporal and spatial resolution (3). The reconstruction of images provides much more information without the degradation of images, and the amount of radiation exposure can also be reduced (4).

The usefulness of MDCT for the evaluation of pediatric disease has been reported. There have been several studies dealing with complicated cardiac anomalies (5), vascular diseases (6), respiratory diseases (7,8), or anorectal malformations (9). However, there have so far been very few studies involving pediatric neoplastic diseases, in particular, regarding liver tumors (10,11). A conventional CT examination and angiography were routinely performed for the preoperative evaluation for liver tumors in many institutions. Repeated CT scans were necessary to evaluate the efficacy of the preoperative chemotherapy. Therefore, serious problems were encountered regarding the accumulation of radiation exposure. On the other hand, general anesthesia is necessary for angiography and it is an invasive procedure for neonates and infants. MDCT more rapidly provides images than does conventional CT, which simplifies the process of sedation, and the MDCT provides a better quality of images and decreases the total accumulated dosage of radiation (12). MDCT also makes it possible to image the precise vascular anatomy including the anomalous branches, feeding arteries, or drainage veins (13).

As shown by the presented cases, the reconstructed images from MDCT were never inferior to those obtained by angiography. Anomalous vessel branches were detected in 3 of the 10 cases and 2 of them were confirmed by the findings by the subsequent angiography. Therefore, when a chemoembolization by TACE is not necessary, this MDCT reconstruction is considered to provide a sufficient evaluation of the vessels.

On the other hand, each image phase (arterial phase, equilibrium phase, portal phase) could be independently and simultaneously extracted or combined, respectively. These combined images can not be obtained by conventional CT procedures.

Furthermore, the software program for volumetry provides a proposed remnant liver volume and an optimal cut line of the liver. Various preoperative simulations can thus be considered. The residual liver volume was calculated to be above 40% for all the presented cases. This volumetric analysis therefore positively contributes to the safety of the procedure by assisting in the selection of the optimal operations.

Since the pediatric age ranges from the neonate to school children having an adult physical constitution, standard-

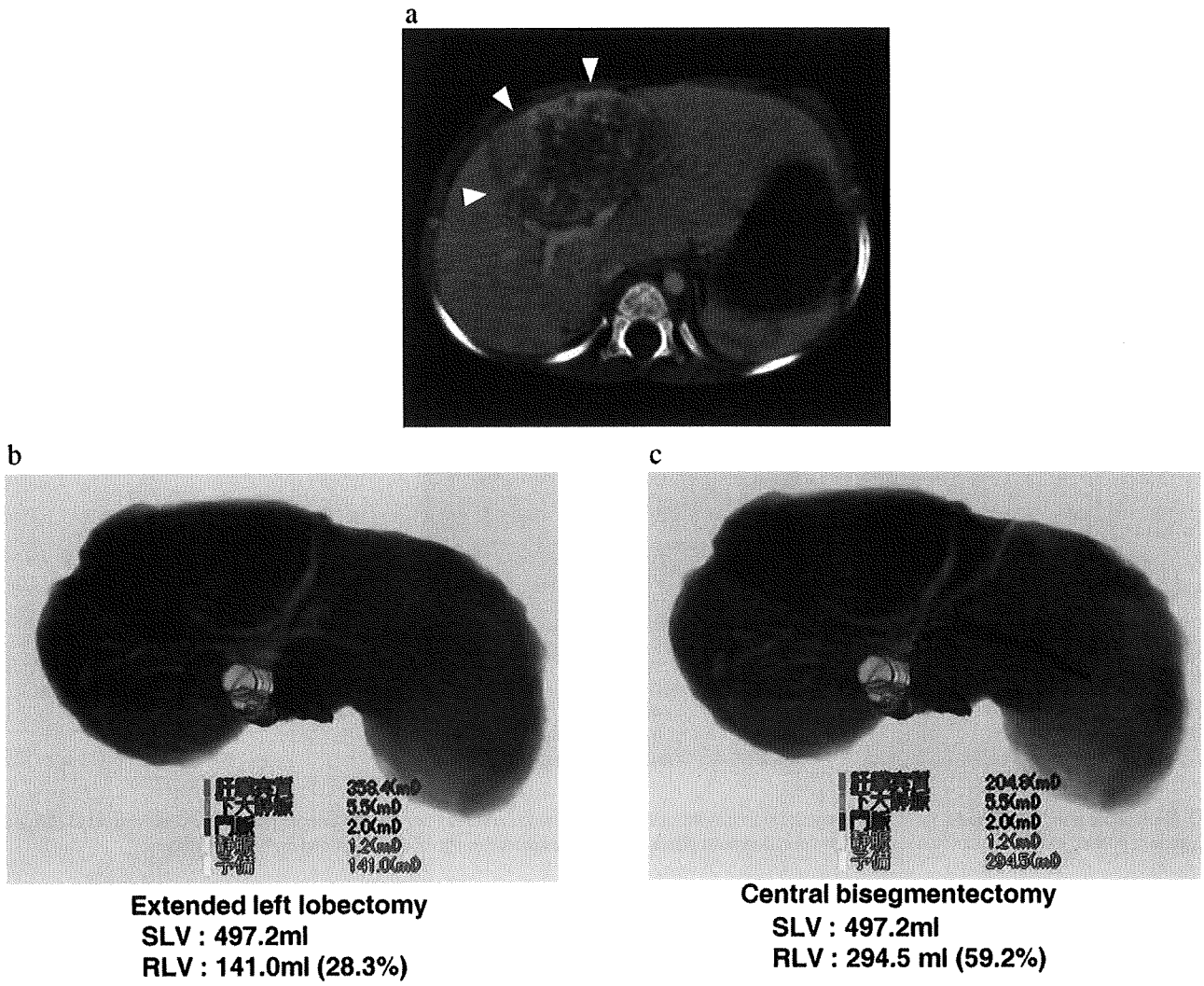

Figure 3. The volumetric analysis (case 2). (a) A 2-D image of a conventional CT scan. (b) The simulation of an extended left lobectomy. The standard liver volume (SLV) was 497.2 ml and the residual liver volume (RLV) was 141.0 ml (28.3%). (c) The simulation of a central bisegmentectomy. The residual liver volume was 294.5 ml (59.2%).

ization of the regimen for each age group is considered to be necessary. Relatively large diameter vessels are necessary for the enhancing procedure, in spite of the difficulty of preserving the vascular route. The volume of the contrast medium, allergic events, and the timing of enhancement are still unsolved problems.

In conclusion, the reconstruction images by MDCT and the performance of a volumetric analysis provide extensive useful information for the preoperative evaluation. Since pediatric surgeons perform these reconstructive procedures themselves, it is possible to obtain the most adequate preoperative evaluation, in order to then select the optimal operation for each patient. The resolution of the specific problems in the pediatric area, and the development of more effective procedures is expected in the future.

Acknowledgements

We would like to thank Mr. Brian Quinn for reading the manuscript. This study was supported in part by a grant-in-aid for scientific research from the Japanese Society for Promotion of Science.

References

1. Yonemura Y, Taketomi A, Soejima Y, *et al*: Validity of preoperative volumetric analysis of congestion volume in living donor liver transplantation using three-dimensional computed tomography. Liver Transpl 11: 1556-1562, 2005.
2. Urata K, Kawasaki S, Matsunami H, *et al*: Calculation of child and adult standard liver volume for liver transplantation. Hepatology 21: 1317-1321, 1995.
3. Rubin GD, Dake MD, Napel SA, *et al*: Three-dimensional spiral CT angiography of the abdomen; initial crinical experience. Radiology 186: 147-152, 1993.
4. Heiken JP, Brink JA and Vannier MW: Spiral (herical) CT. Radiology 189: 647-656, 1993.
5. Westra SJ, Hill JA, Alejos JC, *et al*: Three-dimensional herical CT of pulmonary arteries in infants and children with congenital heart disease. Am J Radiol 173: 109-115, 1999.
6. Chan FP and Rubin GD: MDCT angiography of pediatric vascular diseases of the abdomen, pelvis, and extremities. Pediatr Radiol 35: 40-53, 2005.
7. Siegel MJ: Multiplanar and three-dimensional multi-detector row CT of thoracic vessels and airways in the pediatric population. Radiology 229: 641-650, 2003.

8. Kosucu P, Ahmetoglu A, Koramaz I, *et al*: Low-dose MDCT and virtual bronchoscopy in pediatric patients with foreign body aspiration. Am J Roentgenol 184: 1706-1707, 2005.
9. Watanabe Y, Ikegami R, Takasu K, *et al*: Three-dimensional computed tomographic images of pelvic muscle in anorectal malformations. J Pediatr Surg 40: 1931-1934, 2005.
10. Fuchs J, Warmann SW, Szavay P, *et al*: Three dimensional visualization and virtual simulation of resection in pediatric solid tumors. J Pediatr Surg 40: 364-370, 2005.
11. Dong Q, Xu W, Jiang B, *et al*: Clinical application of computerized tomography 3-D reconstruction imaging for diagnosis and surgery in children with large liver tumors or tumors at the hepatic hilum. Pediatr Surg Int 23: 1045-1050, 2007.
12. Frush DP, Slack CC, Hollingsworth CL, *et al*: Computer-simulated radiation dose reduction for abdominal multidetector CT of pediatric patients. Am J Roentgenol 179: 1107-1113, 2002.
14. Frericks BB, Caldarone FC, Nashan B, *et al*: 3D CT modeling of hepatic vessel architecture and volume calculation in living donated liver transplantation. Eur Radiol 14: 326-333, 2004.